INSTITUTE OF PHYSICS PUBLISHING METROLOGIA
Metrologia **43** (2006) 142–162 doi:10.1088/0026-1394/43/1/020

Acoustic thermometry: new results from 273 K to 77 K and progress towards 4 K

Laurent Pitre[1,2], **Michael R Moldover**[1] **and Weston L Tew**[1]

[1] Process Measurement Division, National Institute of Standards and Technology, Gathersburg, MD 20899-8360, USA
[2] Institut National de Métrologie, Laboratoire National de Métrologie et d'Essai, CNAM, 292 Rue Saint Martin, 75003 Paris, France

E-mail: michael.moldover@nist.gov

Received 22 July 2005
Published 13 January 2006
Online at stacks.iop.org/Met/43/142

Abstract
We used a quasi-spherical cavity as an acoustic and microwave resonator to measure the thermodynamic temperatures, T, of the triple points of equilibrium hydrogen, neon, argon and mercury and to measure the difference $T - T_{90}$, in the range 7 K to 273 K. (T_{90} is the temperature on the International Temperature Scale of 1990 (ITS-90).) In the range 7 K to 24.5 K, our preliminary values of $T - T_{90}$ agree with recent results from dielectric-constant gas thermometry and achieve uncertainties that are comparable to or smaller than those achievable using the interpolating constant volume gas thermometer as currently defined on the ITS-90. In the range 90 K to 273 K, the present results for $T - T_{90}$ obtained using a helium-filled, copper-walled, quasi-spherical cavity agree with earlier results obtained using argon-filled, steel-walled or aluminium-walled, spherical cavities. The agreement confirms our understanding of both acoustic and microwave cavity resonators and demonstrates that resonators function as primary thermometers spanning wide temperature ranges. The mutually consistent acoustic thermometry data from several laboratories imply that the values of $(T - T_{90})/T_{90}$ are 5 times larger than the uncertainty of T/T_{90} near 150 K and near 400 K. They also imply that the derivative $\mathrm{d}T/\mathrm{d}T_{90}$ is too large by approximately 10^{-4} near 273.16 K and that $\mathrm{d}T/\mathrm{d}T_{90}$ has a discontinuity of 4×10^{-5} at 273.16 K.

1. Introduction and prospects

1.1. Overview

We report new acoustic measurements of $T - T_{90}$ in the range $7\,\mathrm{K} < T < T_{\mathrm{w}}$. (Here T is the thermodynamic temperature, T_{90} is the temperature on the (ITS-90), and $T_{\mathrm{w}} \equiv 273.16\,\mathrm{K}$ is the temperature of the triple point of water.) Our results in the range $96\,\mathrm{K} < T < T_{\mathrm{w}}$ are consistent with other recent acoustic determinations of $T - T_{90}$ [1–4]. Our preliminary results in the range $7\,\mathrm{K} < T < 24.5\,\mathrm{K}$ are very close to recent results from dielectric-constant gas thermometry (DCGT) [5]. The good agreement of the present data with prior data increases the confidence in primary acoustic thermometry, particularly because we used significantly different techniques.

We determined the thermodynamic temperature, T, by measuring the pressure dependence of the acoustic resonance frequencies, f_{a}, and of the microwave resonance frequencies, f_{m} of a helium-filled, copper-walled, quasi-spherical cavity using the relation

$$\frac{T}{T_{\mathrm{w}}} = \lim_{p\to 0}\left(\frac{f_{\mathrm{a}}+\Delta f_{\mathrm{a}}}{\langle f_{\mathrm{m}}+\Delta f_{\mathrm{m}}\rangle}\right)^2_{T} \Big/ \lim_{p\to 0}\left(\frac{f_{\mathrm{a}}+\Delta f_{\mathrm{a}}}{\langle f_{\mathrm{m}}+\Delta f_{\mathrm{m}}\rangle}\right)^2_{T_{\mathrm{w}}} = \lim_{p\to 0}(u/c)^2_{T} / \lim_{p\to 0}(u/c)^2_{T_{\mathrm{w}}}. \quad (1)$$

In equation (1), p is the pressure, the subscripts 'a' and 'm' represent the indices that identify particular acoustic and microwave modes, the subscripts 'T' and 'T_{w}' are the temperatures of the measurements, u and c are the measured speeds of sound and of light, respectively, and Δf_{a} and Δf_{m} are corrections to the measured frequencies discussed

below. The relevant microwave resonances occur in closely spaced triplets and the brackets $\langle\cdots\rangle$ denote the average over the three components of the triplet. The second equality in equation (1) follows from the observation by Mehl and Moldover that each corrected frequency ratio is the ratio u/c in that thermodynamic state [6]. In this work, f_a and f_m were measured essentially simultaneously at each temperature and pressure of the gas. Thus, the extrapolation to zero pressure requires the cavity to have stable dimensions *only for the duration of the measurements on each isotherm*. The other properties of the resonator affect the ratio u/c determined via equation (1) by small correction terms. For example, an isotropic expansion of the resonator will not change the ratio u/c; an anisotropic expansion will change the measured ratio u/c in order $(\delta a/a)^2$, where δa is the difference of the expansion of two 'radii' of the quasi-sphere, integrated from T to T_w.

Figure 1 compares the present results with six of the data sets [7–12] that were used to establish the ITS-90 and with four sets of acoustic thermometry data [1–4] that have been published since 1998. The five acoustic data sets are more mutually consistent than the six non-acoustic data sets that helped establish ITS-90. The dashed curve on figure 1 that guides the eye through the acoustic data represents the equation

$$10^6(T/T_{90}-1) = 51[\tanh(2.8(T/T_w-1)+0.5)-\tanh(0.5)]. \quad (2)$$

The lower panel of figure 1 uses equation (2) as a baseline to show that the present results for $(T - T_{90})/T_{90}$ agree with the earlier acoustic thermometry data, nearly within the $k = 1$ uncertainties claimed by the various authors. (Uncertainties are expressed as ks, where s is the standard deviation and k is the coverage factor.) The deviations from equation (2) shown in the lower panel of figure 1 are approximately $(1/5) \times (T - T_{90})/T_{90}$ near 150 K and near 400 K. Thus, a new temperature scale could be five times closer to the thermodynamic temperature than ITS-90 near 150 K and 400 K.

As T_w is approached, the error in $(T-T_{90})/T_{90}$ vanishes by definition; however, the derivative dT/dT_{90} is not constrained to be exactly 1. As figure 2 reveals, $dT/dT_{90} \approx 1.0001$, when averaged over the range 200 K to 375 K. (The solid line in figure 2 passes through T_w and has the slope $dT/dT_{90} = 1.000\,094$.) The departure of dT/dT_{90} from 1 is an error of 0.01% that might be detected by careful flow calorimetry [13] or by careful tests of thermodynamic relationships involving dT/dT_{90}, such as the Clausius–Clapeyron equation. Also, the derivative dT/dT_{90} has a discontinuity of approximately 4×10^{-5}, as illustrated by the dashed lines in figure 2. This discontinuity implies that a standard platinum resistance thermometer (SPRT) that is calibrated at T_w and at the gallium point T_{Ga} will measure temperatures near the mercury point T_{Hg} that are too cold by $4 \times 10^{-5} \times (T_w - T_{Hg}) \approx 1.6$ mK. The discontinuity in dT/dT_{90} had been predicted [14–16] assuming that the resistance ratios of platinum ($W \equiv R_T/R_{273.16}$) are a very smooth function of the thermodynamic temperature, T, and by measuring $W(T_{Ga})$ and $W(T_{Hg})$. In effect, acoustic thermometry has measured $W(T)$ and confirmed that it is indeed smooth.

Figure 3 compares our preliminary values of $(T - T_{90})/T$ in the range 7 K to 24.5 K with gas thermometry data [10–12, 17] used to establish T_{90} and with the results of Fellmuth *et al*'s recent reanalysis of the DCGT data of Luther *et al* [5]. The present results overlap the gas thermometry data and agree with the more precise DCGT results within the small, combined, ($k = 1$) uncertainties. Our data in the range 7 K to 24.5 K were taken in the presence of unanticipated heat leaks resulting from errors in the design of the cryostat (see section 2.4). These design errors will be remedied in the near future; then, our preliminary data will be replaced by new measurements. Taken together, figures 1 and 3 demonstrate that a single, helium-filled cavity can function as a primary thermometer in the range 7 K to T_w. Such a cavity might replace an interpolating gas thermometer and it might reduce the need for low-temperature fixed points.

1.2. Innovations

There are significant differences in technique between this work and previously reported acoustic thermometry; therefore, the agreement of the present results with previous results in the range 96 K to T_w is a strong confirmation of the accuracy of both the theory and the auxiliary data used to determine the corrections Δf_a and Δf_m in equation (1). In this work, the thermometric gas was helium. In contrast, previous acoustic thermometry [1–4] used argon (with the exception of a single isotherm using xenon [1]). The use of different gases is significant because the largest component of the corrections Δf_a in equation (1) accounts for heat exchange between the gas and the metal shell confining it during each acoustic cycle. This term is proportional to $(D_T)^{1/2}$, where D_T is the thermal diffusivity of the gas. At the same temperature and molar density, D_T is approximately 10 times larger in helium than in argon. In this work, the resonant cavity was copper-walled; previous acoustic thermometry used stainless-steel or an aluminium alloy. The use of different metals is significant because the term Δf_m in equation (1) accounts for the penetration of the electromagnetic field into the walls bounding the cavity. The penetration depth varies as $\sigma^{-1/2}$, where σ is the electrical conductivity. The conductivities of copper and stainless steel differ significantly; at 77 K, $\sigma_{copper}/\sigma_{stainless\text{-}steel} \approx 310$; at T_w, $\sigma_{copper}/\sigma_{stainless\text{-}steel} \approx 50$ [18].

The present work demonstrates the utility of quasi-spherical cavities for primary thermometry. (The quasi-sphere is sketched in figure 1 of [19, 23].) The cavity was nearly spherical with a radius of 5 cm. From coordinate metrology, the small departures from sphericity were characterized by $\varepsilon_1 = 0.004\,83$ and $\varepsilon_2 = 0.001\,17$ in the notation of [19]. By design, these departures from sphericity were large enough to separate the triply degenerate TM1n and TE1n microwave modes into three non-overlapping components. It was easy to measure the frequency of each component using a microwave vector analyser. We used the arithmetic average of the three component frequencies for $\langle f_m + \Delta f_m\rangle$ in equation (1). In contrast, previous acoustic studies of ITS-90 used resonators that were as spherical as possible; their values of ε_1 and ε_2 were so small that the components of the microwave modes overlapped each other, complicating the measurement of f_m and increasing its uncertainty.

Previous acoustic thermometry used straight-wire antennas that couple only to the TM microwave modes. As described

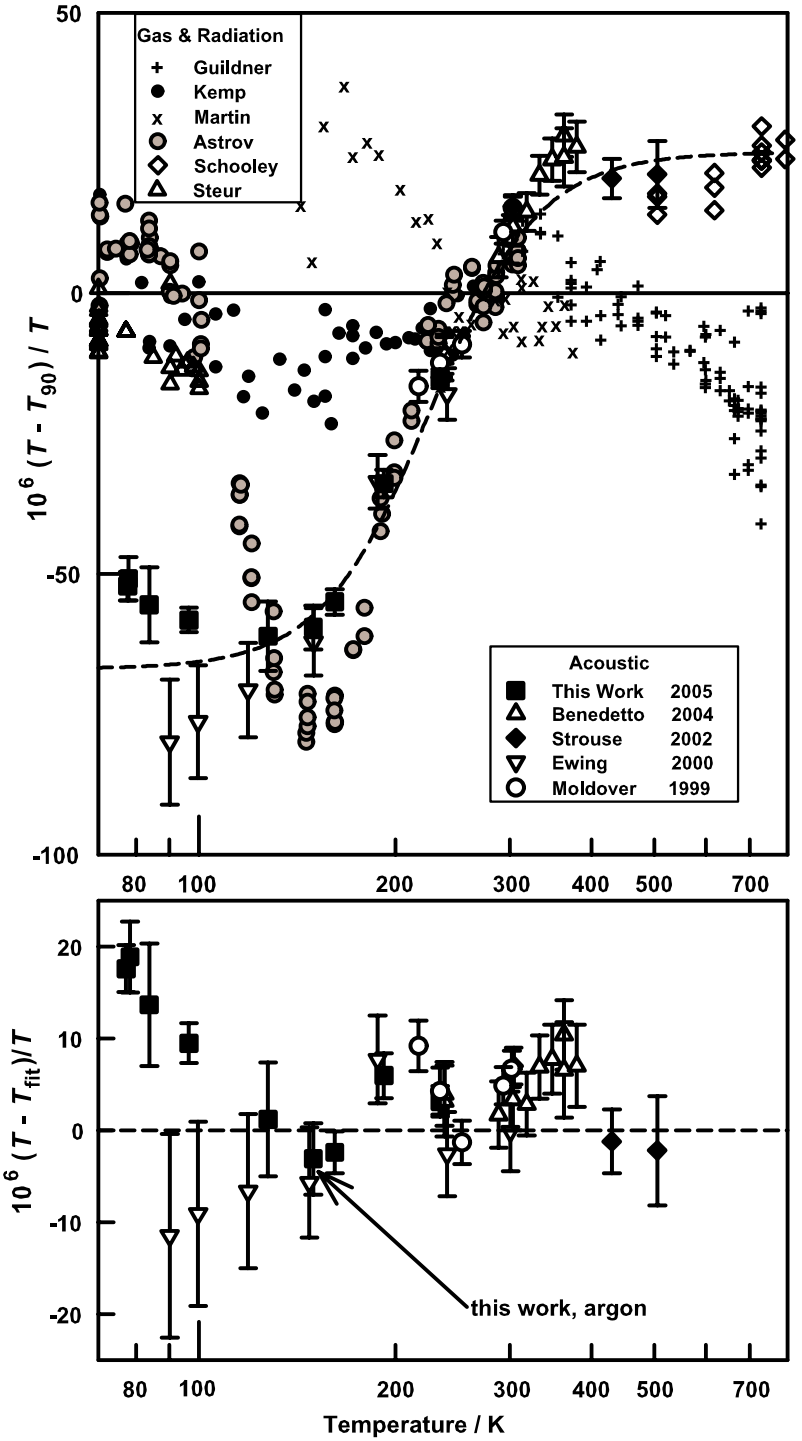

Figure 1. Comparison of present data with data from the literature. The data sources are: Guildner and Edsinger [8]; Kemp *et al* [11]; Martin *et al* [7]; Astrov *et al* [10]; Schooley [9]; Steur and Durieux [12]; Benedetto *et al* [4]; Strouse *et al* [2]; Ewing and Trusler [3]; Moldover *et al* [1]. The dashed curve is a three-parameter fit of equation (2) to the five sets of acoustic data.

in [19], we used judiciously-located coiled loop antennas that allowed us to couple to the TE11 triplet (2.62 GHz) and the TM11 triplet (4.28 GHz). The results for the two triplets were remarkably consistent. At T_w, $\langle (f+g)_{TE11}\rangle / \langle (f+g)_{TM11}\rangle = 1.637\,737$; near 77 K, this ratio decreased by (0.5 ± 0.3) ppm (parts per million). (Here, 'g' $\approx \Delta f_m$ denotes the half-width of the component with frequency f.) The decrease of (0.5 ± 0.3) ppm is a measure of the uncertainty of the resonator's thermal expansion; this uncertainty is a small fraction of the uncertainty of $(T - T_{90})$.

When filled with gas, the quasi-spherical cavity retained the easily-studied, high Q, non-degenerate, radially-symmetric $(0, n)$ acoustic modes of a spherical cavity. In the quasi-sphere, the triply degenerate $(1, n)$ acoustic modes of a spherical cavity were split into three well-resolved components; however, only one of the three components

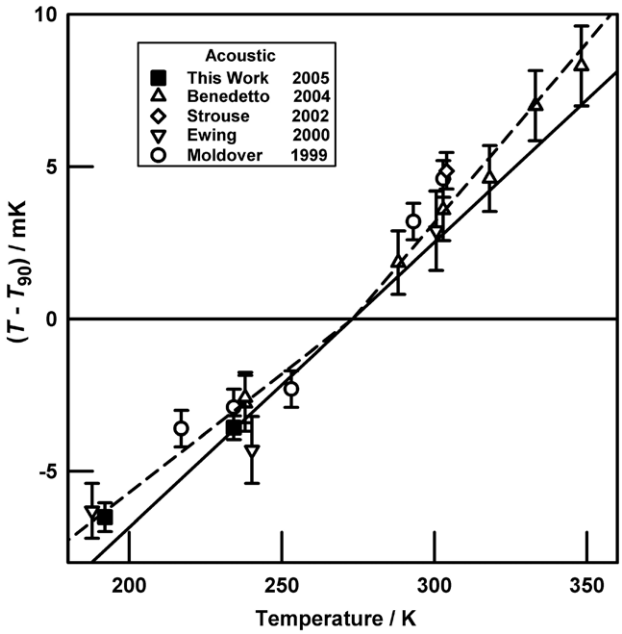

Figure 2. Acoustic thermometry results near T_w. The data sources are Benedetto *et al* [4]; Strouse *et al* [2]; Ewing and Trusler [3]; Moldover *et al* [1]. The solid line is the equation: $(T - T_{90}) = 1.000\,094(T - T_w)$. It was fit to all the data and forced to pass through the point $(T_w, 0)$. The dashed lines are separate fits to the data above and below T_w and forced to pass through $(T_w, 0)$.

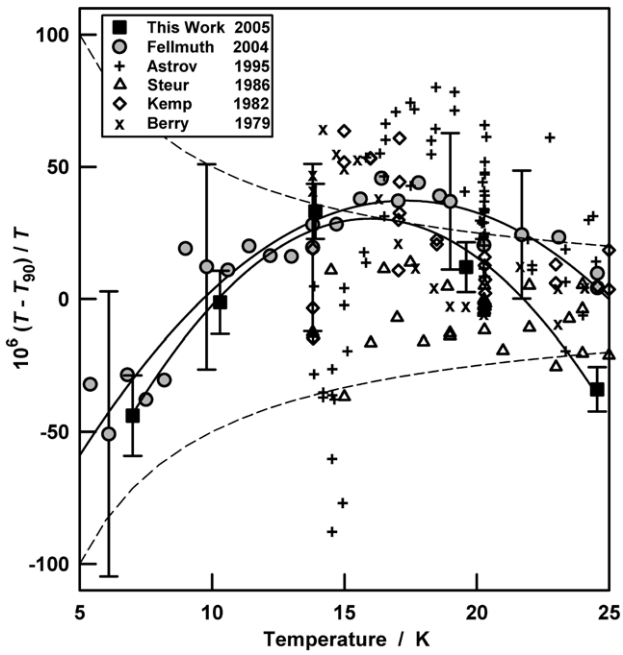

Figure 3. Comparison of present results with data from the literature. The data sources are: Fellmuth *et al* [5]; Astrov *et al* [10]; Steur and Durieux [12]; Kemp *et al* [11]; Berry [17]. The solid curves are quadratic functions of T fitted to 'Fellmuth 2004' and 'This work'. The dashed curves are the 0.5 mK uncertainties of ITS-90.

could be detected because of the locations of the acoustic transducers. In determining the thermodynamic temperature on most isotherms, we gave equal weight to six modes: (0, 3), (0, 4), (0, 5), (0, 6) and to the single detected component each of the (1, 4) and (1, 5) modes. In previous work, only the $(0, n)$ modes were used. The $(1, n)$ modes were particularly useful at temperatures when one of the $(0, n)$ frequencies accidentally coincided with a resonance of the copper shell.

In comparison with argon, the speed of sound in helium is much more sensitive to impurities. We adopted the flowing gas technique of Ripple *et al* [20] to reduce possible contamination from outgassing. By using a liquid-helium-cooled trap, we found evidence of noble gas impurities in the helium, and we accounted for them.

In this work we accounted for the thermoacoustic boundary layer using values for the thermal conductivity of helium calculated using quantum mechanics and statistical mechanics [21, 22][3]. The calculated values have smaller uncertainties than the measured values for any low-density gas. The same calculations provided accurate values of the second acoustic virial coefficient β_a of helium, a quantity that we determined as we took the zero-pressure limit in equation (1). Within small combined uncertainties, our measured values of β_a agree with the calculated values. This consistency provides extra confidence in the present results.

1.3. Prospects for improvement

The results presented here may be improved by several changes in the apparatus. We discovered that when the bath was filled with helium and the resonator was much warmer than the bath, extra noise appeared in the acoustic signals. (The bath surrounded the vacuum can, heat shield and pressure vessel, as sketched in figure 4.) This noise discouraged us from acquiring data between 25 K and 77 K. We suspect that the noise was generated by boiling of the helium bath forced by the 'warm' gas returning from the resonant cavity through an 8 mm diameter tube that passed through the bath. As boiling occurs, the pressure in the tube fluctuates, causing adiabatic temperature (and speed of sound) fluctuations in the gas within the resonant cavity. We expect that insulating the gas-return tube from the bath will enable measurements of $(T - T_{90})$ between 25 K and 77 K. Second, we learned that the acoustic modes were significantly perturbed by the coil-terminated coaxial cables that coupled microwaves into and out of the cavity. Because these perturbations are hard to estimate, we shall place the coils behind a dielectric window located flush with the interior surface of the cavity, thereby eliminating the perturbations to the acoustic modes. Third, the interior surface of the resonator was left in an as-machined condition to avoid changing its quasi-spherical shape in an uncontrolled manner. We shall electropolish this surface. We hope that this will reduce the apparent precondensation of argon that we observed at 95 K and of helium that we observed at 4 K. Electropolishing this surface may also reduce the excess half-widths of the microwave resonance frequencies, particularly at low temperatures. We are no longer so concerned about the shape of the quasi-sphere because we discovered that the present quasi-sphere makes a satisfactory primary thermometer, even though its departures from sphericity are much larger and more complicated than our design.

[3] Reference [21] tabulates the properties of helium calculated from the potential ϕ_{00}, and defines the potential ϕ_B. Subsequent work [20] shows ϕ_B is more nearly consistent with the most recent *ab initio* calculations; thus, we used properties calculated from ϕ_B.

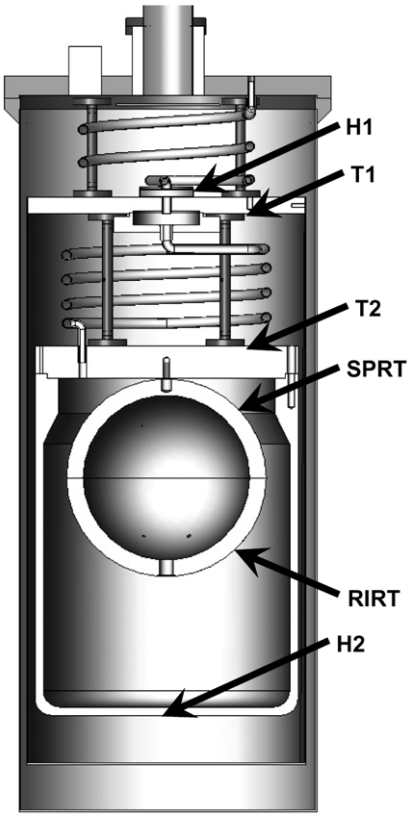

Figure 4. Cross-section of the resonator, pressure vessel, heat shield and vacuum can. Thermometer T1 and heater H1 regulated the temperature of the heat shield. Thermometer T2 measured the temperature of the top of the vacuum can. Heater H2 was used to warm the can following reductions of the gas pressure. 'RIRT' and 'SPRT' indicate the locations of the RIRT and the capsule-type SPRT.

Finally, we found that the extrapolation of equation (1) to zero pressure had significant uncertainties at low temperatures from the uncertainties of the higher acoustic virial coefficients of helium that we took from the literature. In the future, we will re-determine these virial coefficients ourselves by extending the acoustic measurements to higher densities. The existing apparatus has this capability.

2. Apparatus and procedures for determination of T

2.1. Resonator

Our quasi-spherical resonator was designed by Mehl *et al* to simplify the microwave measurements associated with acoustic thermometry [19]. NIST's Fabrication Technology Division manufactured two nominally-identical resonators from a single billet of oxygen-free, high-conductivity copper (OFHC). Each resonator was assembled by bolting together two, nearly-identical, quasi-hemispherical shells. Each shell had nominal inside and outside radii of 5 cm and 6 cm, respectively. May *et al* [23] characterized the resonator used in this work. They found the shells had small departures from sphericity that were characterized by $\varepsilon_1 = 0.004\,83$ and $\varepsilon_2 = 0.001\,17$ in the notation of [19]. The value of ε_1 was five times larger than our design and the shape was more

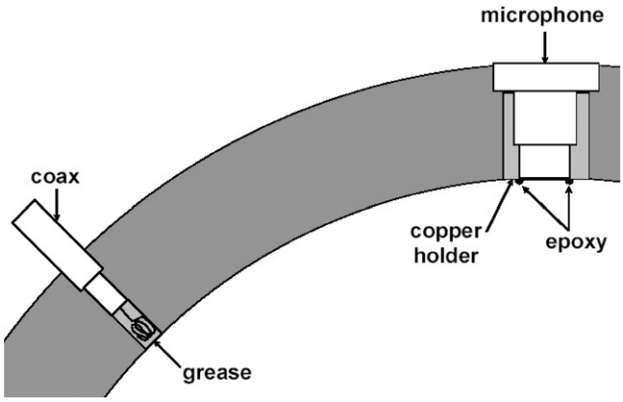

Figure 5. Cross-section of quasi-sphere showing locations of microwave antenna and microphone.

complicated than intended [23]. Nevertheless, the resonator was entirely satisfactory for acoustic thermometry. This demonstrates that the design concepts are robust.

Six holes were drilled radially through the quasi-spherical shell used in this work. The angular locations of the holes are specified in spherical polar coordinates by polar and azimuthal angles (θ, φ) (figure 1 of [19] and [23]). The polar (z) axis coincides with the largest 'radius' of the quasi-sphere and the azimuthal axis (x) coincides with second largest 'radius'. Holes at (39°, 0°) and (0°, north pole) held the acoustic transducers; holes at (45°, 45°) and (135°, 135°) admitted coaxial cables for the microwave measurements; one hole at (180°, south pole) accepted the duct that supplied gas to the cavity, and the sixth hole at (45°, 90°) accepted the duct that exhausted gas from cavity. Figure 5 shows an acoustic transducer and a microwave cable installed in their respective holes.

2.2. Acoustic transducers and cables

The acoustic transducers were commercially manufactured capacitor microphones[4,5]. As sketched in figure 5, the microphones were installed so that their metal diaphragms were nearly flush with the inner surface of the cavity. We found that the microphones increased the half-widths of the microwave resonances. For example, at 295 K, the values of $10^6\, g/f$ of the three components of the TM11 mode were 19.5, 19.5 and 21.8. When the microphones were replaced by clean OFHC copper plugs, these values decreased to 18.4, 18.3 and 21.5, respectively. Perhaps this small change in g/f and its possible temperature dependence could be calculated from the conductivity and the magnetic susceptibility of the diaphragm. We did not attempt this because other uncertainties were much larger.

Coaxial cables led from an audio-frequency synthesizer to an amplifier and then to the transducer that generated sound. This transducer was biased with 100 V (dc) and it was driven

[4] Bruel and Kjaer Model 4938.

[5] In order to describe materials and experimental procedures adequately, it is occasionally necessary to identify commercial products by manufacturers' name or label. In no instance does such identification imply endorsement by the National Institute of Standards and Technology, nor does it imply that the particular product or equipment is necessarily the best available for the purpose.

by a sinusoidal voltage 20 V (RMS). The detector microphone was biased by a battery at 132 V dc. A coaxial cable led from the detector-microphone to a lock-in amplifier that was operated in the current mode. The current mode is often used in cryogenic apparatus [24] to detect signals from capacitive sources because it does not require triaxial cables that are difficult to thermally anchor. However, in the current mode, the detected signal decreases as $1/f$. In our installation, there was significant electrical crosstalk from the drive circuit to the detector circuit. Because of the crosstalk, we altered the traditional protocol for acquiring and fitting the acoustic resonance data, as described in section 2.6.

2.3. Microwave transducers and cables

Coaxial cables led from the microwave vector analyser to 2.3 mm diameter ducts that had been drilled through the walls of the cavity. The manufacturer stated that the cables had a $0.086''$ outer diameter ($1'' = 2.54$ cm) copper conductor and a silver-plated inner conductor (Microstock Inc., type 85SP-0790-30STP)[5]. Each cable was terminated by a coupling coil, as sketched in figure 5 and as described in [19]. Each coil had a diameter of approximately 2 mm and was made of three turns of 0.43 mm diameter copper wire. While in their ducts, the coils were rotated until the detected signal near the resonance frequency of the TM11 mode was as large as possible. The coils were recessed in the ducts approximately 2 mm beneath the inner surface of the cavity. This location was selected by measuring the decrease of g_{TE11} with distance while each coil was withdrawn from the cavity. (g_{TE11} is the half-width of the TE11 mode.) The withdrawal was halted when the decrease of g_{TE11} became too small to measure. We sealed the outer conductor and the insulation of the cables in the duct with a bead of Stycast 2850 FT epoxy[5]. The epoxy filled the crevice between the outer conductor and the duct, and it retarded gas exchange between the cavity and the cable's insulation.

We discovered that the coupling coils and their ducts significantly increased the half-widths of the acoustic resonances. This discovery solved the puzzle of excess half-widths described in [19]. We reduced the excess half-widths by partially filling the ducts with vacuum grease (Apiezon N Cryogenic High Vacuum Grease[5]). For example, when the resonator was filled with argon at low pressures at T_{w}, $\Delta g/f$ was 12 ppm, 28 ppm and 32 ppm for the (0, 3), (0, 4) and (0, 5) acoustic modes before applying the grease. After applying the grease, $\Delta g/f$ was 13 ppm, 6 ppm and 3.5 ppm, under the same conditions. (Here, $\Delta g \equiv g_{\mathrm{meas}} - g_{\mathrm{calc}}$ is the difference between the measured half-widths and those calculated using the theory from [25].) We did not fill the ducts completely with grease because we feared that the grease might migrate into the microphones. In the future, we will cover the coupling coils with dielectric windows that seal the ducts at the inner surface of the cavity.

2.4. Cryostat

Figure 4 shows the resonator and the surrounding metal shells. The resonator was enclosed by a pressure vessel (gold-plated copper, 7 mm thick, 20 cm high, 7 cm inner radius). The pressure vessel was enclosed by a heat shield (gold-plated copper, 1 mm thick, 34 cm high, 8 cm inner radius). The heat shield was enclosed by a stainless-steel vacuum 'can' that was immersed in a bath of either ethanol (273 K, 231 K), liquid nitrogen ($77\ \mathrm{K} < T < 192\ \mathrm{K}$) or liquid helium ($7\ \mathrm{K} < T < 24\ \mathrm{K}$). The thermal links between the resonator and the pressure vessel and between the pressure vessel and the heat shield were intentionally weak to shield the resonator from external temperature gradients.

Usually, we regulated the temperature of the heat shield using the auxiliary thermometer T1 and the heater H1 (figure 4). The largest temperature gradients occurred while the heat shield was maintained at 161 K and the vacuum can was immersed in liquid nitrogen at 77 K. In this configuration, the top of the heat shield was 50 mK warmer than the top of the pressure vessel, as indicted by thermometers T1 and T2. Under these conditions, a heat conduction model predicted that the top of the shield was also 50 mK warmer than the bottom of the shield and the top of the resonator was only 0.15 mK warmer than its bottom. We tested the conduction model by applying 5 mW to a heater H2 on the bottom of the pressure vessel while monitoring a thermometer on the resonator and a resonance frequency. The frequency tracked the temperature within the resolution of the measurements, which was equivalent to 1 ppm of the frequency or 2 ppm of the temperature.

On each isotherm, the frequency, temperature and pressure were measured under near-equilibrium conditions. During these measurements, the heater H2 was off, the temperature of the heat shield was controlled by T1 and H1 and the temperature of the resonator 'floated'. When the measurements were completed, the pressure was stepped downward and the adiabatic expansion of the gas cooled the resonator and the pressure vessel. Immediately after each pressure step, we used the heater H2 to warm the bottom of the pressure vessel. After a few minutes, the pressure vessel's temperature returned to the temperature of the heat shield. Then, we turned off the heater and waited until the temperature transients decayed. At T_{w}, we took data stepping the pressure both up and down; the results did not depend upon the direction of the step.

We encountered two problems associated with heat transfer. First, the wires that connect the heater on the top of the heat shield to its power supply were too large to be completely thermally anchored to the top of the vacuum can. This caused a large heat leak from the room to the heat shield. When the bath was at 4.2 K and the can was evacuated, the shield temperature approached 7 K; therefore, we could not measure T/T_{w} below 7 K while the can was evacuated. When the can contained exchange gas, the resonator cooled to 4.2 K. We conducted exploratory frequency measurements at 4.2 K; however, the temperature regulation was poor. When the exchange gas was pumped away, the temperature of the heat shield rose. The temperature of the resonator followed the shield's temperature but never exceeded it. This observation indicates that the heat shield and the pressure vessel protected the resonator from the heat conducted by the oversized wires. In the future, we shall replace the oversized wires to enable measurements below 7 K.

The second heat-transfer problem may have resulted from the tube that exhausted helium from the pressure vessel to the room. A section of this tube (8 mm diameter, 1 m long) was coiled in the space between the top of the heat shield and the flange on top of the vacuum can. The heat shield maintained

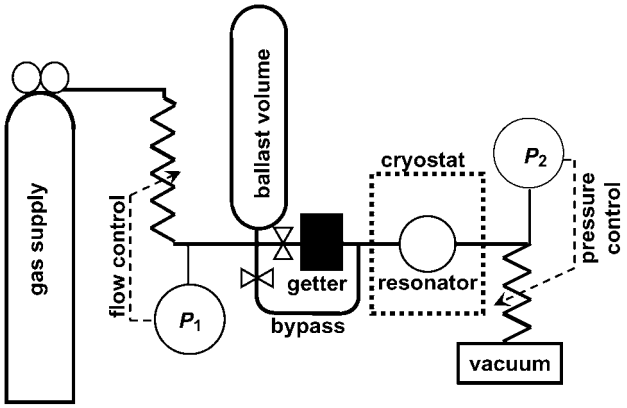

Figure 6. Schematic diagram of gas management system. The pressure sensor P_1 was used to control the flow rate. The pressure gauge P_2 was used to control the pressure in the resonator.

the lower end of this section at the resonator's temperature. The bath maintained the upper end of this section at 4.2 K. When the resonator was between 7 K and 77 K, convection occurred in the tube, boiling occurred in the bath and extra noise appeared in the acoustic signals. As the resonator's temperature was raised, the noise increased and it discouraged us from acquiring data between 25 K and 77 K. We suspect that the noise was generated by pressure fluctuations associated with the boiling and/or convection. Pressure fluctuations in the tube will cause temperature and speed-of-sound fluctuations in the gas in the resonant cavity. If this diagnosis is correct, insulating the inlet and exhaust tubes from the bath will enable measurements of $(T - T_{90})$ between 25 K and 77 K.

2.5. Gas management system

The system for managing helium (and argon) was designed with two circumstances in mind: (1) the speed of sound in helium is very sensitive to impurities and (2) we chose to use polymer-insulated coaxial cables and non-bakeable acoustic transducers. We used non-bakeable components because they enabled us to easily test various experimental arrangements. However, this simplicity introduced the risk of contaminating the helium by virtual leaks or by outgassing from the cables, cable insulation, acoustic transducers, epoxy and vacuum grease, all of which were exposed to the cavity.

In concept, the gas management system resembled that used by Ripple *et al* [20]. A gas manifold at ambient temperature delivered helium to the cryostat at a controlled pressure and flow rate (see figure 6).

Helium flowed through from the manifold at ambient temperature to the resonator through three tubes in succession. The first tube was 2.5 m long and had a diameter of 0.635 mm. The second passed through the temperature gradient in the cryostat; it was 1 m long and had a diameter of 1.27 mm. The third, called the supply duct, was fastened to the cavity. It was 50 mm long and had a diameter of 0.508 mm. The length of the supply duct was chosen to decouple the acoustic resonances of the cavity from unintentional acoustic resonances in the longer tubes. Most of the helium in the cavity flowed out through an exhaust duct (50 mm long, 1.0 mm inside diameter) into the pressure vessel (volume ≈2 L) surrounding the resonator. From the pressure vessel, the helium flowed through a low impedance tube (10 mm diameter from the pressure vessel to the shield and then 8 mm diameter) to a pressure transducer at room temperature and then to a back-pressure regulator and a vacuum pump.

The flow impedance of the exhaust duct was comparatively high. When flow was present, the pressure inside the cavity was higher than the pressure in the vessel surrounding it. Some of the helium leaked from the cavity through the unsealed joint where the quasi-hemispheres contacted each other, and some helium may have leaked out by the transducers and microwave coupling probes. This leakage tended to sweep gases evolving from the cables and transducers out of the cavity.

Precautions were taken to ensure that the gas flow to and from the resonator did not change the resonator's temperature. Figure 4 shows the coiled gas-return line passing through three temperature-controlled surfaces: (1) the top of pressure vessel, (2) the top of heat shield and (3) the flange on top of the vacuum can into the space filled by the bath. The gas-return line was thermally anchored to these three surfaces by heat sinks composed of copper wires. Similar heat sinks were attached to the gas-supply lines. From the top of the vacuum can, the long, thin-walled supply and return lines passed through the bath and through a vapour-filled space above the bath to room temperature. Because the flowing gas exchanged heat with the vapour surrounding the lines, the heat transported by the flowing gas from room temperature to the vacuum can was very small. The measured resonance frequencies were independent of the gas flow rate, confirming that the heat sinking was satisfactory.

The manufacturer of the gases specified upper bounds to the concentration of specific impurities in parts per million by mole fraction. For helium, these bounds were: $O_2 < 1$; $H_2O < 0.2$; total hydrocarbons < 0.1; $CO < 0.1$; $CO_2 < 0.1$; $Ar < 0.5$; $N_2 < 1$; for argon, these bounds were: $O_2 < 0.2$; $H_2O < 0.5$; total hydrocarbons < 0.2; $CO < 0.5$; $CO_2 < 0.5$; $N_2 < 3$. These impurity concentrations are too high for the present work with helium; therefore, we installed a heated metal getter in the helium supply manifold. The manufacturer of the getter specified that it reduced the impurity content to less that 0.01 ppm for reactive gases including H_2O, H_2, O_2, N_2, NO, NH_3, CO, CO_2, CH_4, CF_4, CCl_4 and SiH_4. We made some speed-of-sound measurements on every isotherm above 77 K both with and without passing the helium over the hot getter. For example, the speed of sound increased 3 ppm at T_w when the getter was used.

Noble gas impurities in the helium supply are a concern when determining T/T_w at low temperatures. For example, 1 ppm of neon in the helium will decrease the speed of sound 2 ppm at T_w; however, neon freezes out as the gas flows towards the resonator at, for example, 7 K. If neon was ignored, the value of T/T_w from equation (1) would be 4 ppm too high at 7 K. Similarly, 1 ppm of argon in helium will decrease the speed of sound by 4.5 ppm and decrease the apparent temperature by 9 ppm. In contrast, 1 ppm of helium or neon in argon increases the speed of sound in argon less than 1 ppm. (The comparative insensitivity of argon to impurities is one reason why argon was used in previous acoustic thermometry.)

Because of the sensitivity to impurities, the gas manifold downstream from the heated getter was made entirely from

metal components. The joints were solder or compression fittings, with the exception of one small epoxy joint in the cryostat.

The chance for contaminating the gas inside the resonator by outgassing was greatest during the measurements on the higher-temperature isotherms (192 K to 273 K). Therefore, at these temperatures, we routinely used helium flows in the range 20 µmol s^{-1} to 100 µmol s^{-1}. At 273 K and 600 kPa, the lowest flow replaced the gas in the cavity in 90 min; the highest flow replaced the gas in 22 min. Under these conditions, the resonance frequencies were independent of the flow rate within an uncertainty of 0.74 ppm. This uncertainty contributes to the uncertainty of T and it is included in table 9 under the column 'impurity'. At lower pressures, the resonance frequencies were also independent of the flow rate; however the uncertainty of the tests was larger: 2.5 ppm.

As an additional test for contamination, we stopped the helium flow and monitored the resonance frequencies. The pressure transient generated by stopping the flow generated a temperature transient. After the transients had decayed, the resonance frequency was monitored for several hours. It did not change within the uncertainty of the measurement, indicating that there was no appreciable contamination from outgassing.

2.6. Determining acoustic and microwave resonance frequencies

We determined the acoustic resonance frequencies from measurements of the complex current $\boldsymbol{I}(f) \equiv x + \mathrm{i}y$ generated by the detector microphone as a function of the driving frequency. We fitted the data to the resonance function:

$$\boldsymbol{I}(f) = \frac{\boldsymbol{A}f}{f^2 - \boldsymbol{F}_\mathrm{a}^2} + \boldsymbol{B} + \boldsymbol{C}f. \tag{3}$$

Here, $\boldsymbol{A}, \boldsymbol{B}$ and $\boldsymbol{C}$ are complex constants, and the complex acoustic resonance frequency is $\boldsymbol{F}_\mathrm{a} \equiv f_\mathrm{a} + \mathrm{i}g_\mathrm{a}$. The terms $\boldsymbol{B} + \boldsymbol{C}f$ in equation (3) were more important in this work than in prior work because of the electrical crosstalk between the generator and detector circuits. After examining both simulated and real data, we selected the following protocol for acquiring $\boldsymbol{I}(f)$ data. The drive frequency was stepped across the range $0 < |f - f_\mathrm{a}| < g_\mathrm{a}$ in 20 equal steps of $g_\mathrm{a}/10$, and the current $I(f)$ was measured at each step. Ten additional steps of g_a were made to span the wider range $g_\mathrm{a} < |f - f_\mathrm{a}| < 6g_\mathrm{a}$. At every step, $I(f)$ was integrated for the same time, typically 0.3 s.

At a typical value of the helium density (200 mol m^{-3}), each determination of $\boldsymbol{F}_\mathrm{a}$ had a repeatability of 0.2 ppm. When isotherms were repeated, the values of $\boldsymbol{F}_\mathrm{a}$ were reproduced within approximately 0.9 ppm. The irreproducibility of the temperature and the pressure accounts for the difference between 0.2 ppm and 0.9 ppm.

We determined the microwave resonance frequencies by measuring the complex parameter $\boldsymbol{S}_{12}(f)$ using a microwave vector analyser.

The vector analyser recorded $\boldsymbol{S}_{12}(f)$ in an 8 MHz wide frequency band for TM11 and a 6 MHz band for TE11. The data were fitted by the complex sum of three resonance functions:

$$\boldsymbol{S}_{12}(f) = \sum_{i=1}^{3} \frac{\boldsymbol{A}_i f}{f^2 - \boldsymbol{F}_i^2} + \boldsymbol{B} + \boldsymbol{C}f + \boldsymbol{D}f^2. \tag{4}$$

The average of the three values of $\mathrm{Re}(\boldsymbol{F}_\mathrm{m})$ was taken to be the resonance frequency of the mode under study and is denoted by $\langle f_\mathrm{m} \rangle$ in equation (1). For the TE11 mode, the fractional repeatability of $\langle f_\mathrm{m} \rangle$ was 1 part in 10^8 for $T > 77$ K. For $T < 77$ K, the microwave power was reduced by a factor of 10 to reduce the heating of the resonator. At the reduced power, the repeatability was 3 parts in 10^8. In equation (4), the terms $\boldsymbol{B}+\boldsymbol{C}f+\boldsymbol{D}f^2$ were all significant; this is not surprising because the $\boldsymbol{S}_{12}(f)$ data span a comparatively wide range.

A single quartz crystal oscillator provided the frequency reference for the audio-frequency synthesizer and the microwave vector analyser. Thus, an error in the clock does not cause an error in T/T_w calculated via equation (1).

3. Thermometers and procedures for measurement of T_{90}

One of the principal results of the present work is the determination of values of $(T - T_{90})$. This section describes the techniques used to realize T_{90} in the apparatus and to determine the uncertainty of the realization. In this section, we express uncertainties with the coverage factor $k = 2$, thereby following the custom of the community using resistance thermometers. This custom contrasts with the use of $k = 1$ by the acoustic thermometry community and followed by us elsewhere in this manuscript.

3.1. Resistance thermometers

Temperatures on the ITS-90 were determined in the range 77 K to 273 K by measurements of a capsule type SPRT, serial number 1842382. Temperatures in the range 4 K to 24.56 K were determined by measurements of a rhodium iron resistance thermometer (RIRT), serial number A129.

3.2. ITS-90 SPRT calibration

The SPRT 1842382 has been used for scale maintenance and research purposes at NIST for approximately 25 years. It has remained stable during this time and exhibits exceptionally small deviations ΔW which are negative for all temperatures over the calibration range. The thermometer was first used by Furukawa in 1979 for realizations of the argon triple point [26]. This thermometer was later used by Furukawa [27] in 1985 for determination of the oxygen triple point on the IPTS-68.

Contemporary fixed point realizations with SPRT 1842382 began in 2002 and continued through 2003 and in 2004 just prior to, during and immediately following the acoustic temperature measurements reported here. The repeatability at the triple point of water, including that following excursions to 700 kPa inside the resonator, was in general within ±0.2 mK. Table 1 is a summary of the fixed point calibration data used in the determination of T_{90} above 77 K, listing W values and their associated expanded ($k = 2$)

Table 1. Fixed point calibration data for SPRT 1842382.

Fixed point, T_{90}/K	W (0 mA)	$U(W)$ $k = 2$	ΔW/mK	References
Ga MP, 302.9146	1.118 136 97	4.8×10^{-7}	−0.49	[28]
Hg TP, 234.3156	0.844 140 79	6.4×10^{-7}	−0.34	[29]
Ar TP, 83.8058	0.215 854 34	7.4×10^{-7}	−1.3	[26]
O_2 TP, 54.3584	0.091 707 93	4.0×10^{-7}	−2.6	[27]

MP = melting point, TP = triple point.

Table 2. Deviation function coefficients for SPRT 1842382.

Calibration sub-range	a	b	c_1
83.8058 K to 273.16 K	$8.490\,199\,563 \times 10^{-6}$	$1.043\,779\,276 \times 10^{-6}$	—
54.3584 K to 273.16 K	$9.515\,997\,89 \times 10^{-6}$	$9.670\,909\,89 \times 10^{-6}$	$-1.653\,768\,23 \times 10^{-6}$

uncertainties $U(W)$. Table 2 is a summary of the deviation function coefficients for two ITS-90 defined calibration sub-ranges: 83.8058 K to 273.16 K ('sub-range 4') and 54.3584 K to 273.16 K ('sub-range 3').

All data shown here reflect zero current extrapolations and corrections for known pressure heads in the case of gallium and mercury. The gallium data were derived from contemporary triple point realizations using a NIST Ga cell 'Ga921' [28] but were not necessary for this work and are provided here for reference only. Mercury triple point data are derived from contemporary realizations using a recently-distilled NIST mercury TP cell 'GC-1' [29]. The argon TP data are derived from contemporary realizations using the sealed triple-point cell (STPC) 'Ar-NBS-3' [26]. The oxygen triple point data are derived from archival realizations using the STPC 'PO-3' [27] together with contemporary comparison results [30].

The non-uniqueness in the interpolation of temperature due to inconsistencies of these two ITS-90 sub-ranges is a maximum of 0.21 mK for temperatures in the approximate range 115 K to 135 K. The error due to extrapolation of the 83.8058 K to 273.16 K calibration down to 77.8 K is approximately 0.1 mK.

3.3. ITS-90 RIRT calibration

The RIRT A129 has been used for scale maintenance purposes at NIST for approximately ten years. It was originally calibrated on the ITS-90 between 0.65 K and 24.5561 K using NIST realizations of: ^{3}He vapour pressures, ^{4}He vapour pressures [31] and interpolating constant volume gas thermometer (ICVGT) [32] definitions. This thermometer was one of two submitted by NIST for the Key Comparison 1 (K1) organized by the Consultative Committee for Thermometry (CCT) in 1996, the results of which have recently been published [33].

The RIRT A129 has been periodically compared with other NIST reference RIRTs and shows good agreement with those RIRTs over the entire range of 0.65 K to 24.5561 K [34]. The thermometer's stability has also been verified through contemporary realizations of the Ne TP at NIST.

Temperature is interpolated via a sixth order polynomial fit to the ICVGT data. The polynomial represents resistance R_{A129} as a power series in the temperature T_{90} according to

$$R_{A129}(T_{90}) = \sum_{n=0}^{6} j_n T_{90}^n. \qquad (5)$$

Table 3. Polynomial coefficients for RIRT A129 for temperatures derived from ICVGT realizations.

Coefficient	Value
j_0	2.610 722 989
j_1	0.471 809 956
j_2	−0.027 839 435
j_3	0.001 330 609
j_4	$-4.361\,08 \times 10^{-5}$
j_5	$8.476\,87 \times 10^{-7}$
j_6	$-7.076\,09 \times 10^{-9}$

A summary of the RIRT A129 polynomial coefficients j_n in the ICVGT range is given in table 3. This interpolation equation and the coefficients j_n are the same as was used for this thermometer in K1 over the range 5 K to 24.556 K.

Some non-uniqueness has been observed [35] in the range 13.8 K to 24.5561 K when comparing temperatures derived from the NIST ICVGT realization against those derived from an SPRT sub-range calibration from 13.8 K to 273.16 K when equilibrium hydrogen (e-H_2) vapour pressure realizations are used for the 17 K and 20.3 K calibration points. However, this non-uniqueness is negligible at the particular temperatures chosen in this work.

3.4. Resistance measurements

The resistance thermometers were measured using an ac resistance bridge based on an inductive-voltage-divider operating at 30 Hz. The measurement bandwidth was 0.1 Hz, yielding a least-count resolution of 5×10^{-9} in the resistance ratio. Resistance standards of 100 Ω and 25 Ω were used for the SPRT and RIRT measurements, respectively. These standards were calibrated through other NIST reference resistors traceable to the NIST as-maintained ohm and maintained in a 25 °C oil bath. The bridge linearity was verified to be within the nominal tolerance of $\pm 1 \times 10^{-7}$ of the measured ratio through use of a Hamon-type resistance network device [36].

3.5. ITS-90 uncertainty

3.5.1. SPRT range: 77 K to 273.16 K. The uncertainties shown in table 4 are for the capsule SPRT at each of the calibration fixed points necessary for the two ITS-90 sub-range definitions. The cell types listed are either of two

Table 4. Components of uncertainty in millikelvin for the calibration of SPRT 1842382.

	STPC		IC	
Cell types	O_2TP	Ar TP	Hg TP	H_2O TP
Type A				
Repeatability of realizations with 1842382	0.04	0.05	0.06	0.1
Repeatability of resistance measurement	0.02	0.02	0.02	0.02
Total A	0.045	0.054	0.063	0.102
Type B				
Realizations				
Chemical impurities	0.012	0.050	0.010	0.040
Isotopic variations				0.030
Static-head correction			0.041	0.005
Heat leaks/immersion	0.020	0.020	0.007	0.015
Thermal equilibrium	0.010	0.020	0.020	0.020
Measurement				
Normal bridge accuracy	0.004	0.009	0.005	0.005
Quadrature errors	0.005	0.005	0.001	0.001
Resistance standards	0.016	0.035		
SPRT self-heating	0.003	0.016	0.007	0.01
Total type B	0.031	0.070	0.048	0.057
Total standard uncertainty ($k = 1$)	0.054	0.088	0.080	0.117
Total expanded ($k = 2$)	0.108	0.176	0.159	0.234

types: (a) STPC or (b) immersion cells (IC). Immersion cells generally have pressure head corrections while STPCs generally do not.

Using the fixed point calibration uncertainties, the calibration uncertainty $U_c(T)$ is calculated as the root sum square (RSS) of the individual fixed point uncertainty contributions as propagated over the calibration sub-range. Uncertainty in the measurement of ITS-90 temperatures using the calibrated SPRT must also include a component $U_{wtp}(T)$ for the propagation of the water triple point uncertainty. In addition, for the purposes of this work, we include a contribution $U_{nu}(T)$ which represents the non-uniqueness from sub-range inconsistencies. The total uncertainty U_{90} in the T_{90} temperatures is the RSS of these three principal components. These contributions are shown in figure 7. The uncertainty values are also shown in table 5 for the temperatures compared in this work.

3.5.2. ICVGT range: 5 K to 24.5561 K. The uncertainties for the calibration of RIRT A129 as derived from the NIST realization of the ICVGT are shown in table 6. The total expanded uncertainties for the specific temperatures compared in this work are given in table 7. The polynomial fit residuals are shown in figure 8 together with the upper and lower bounds of the total expanded uncertainty.

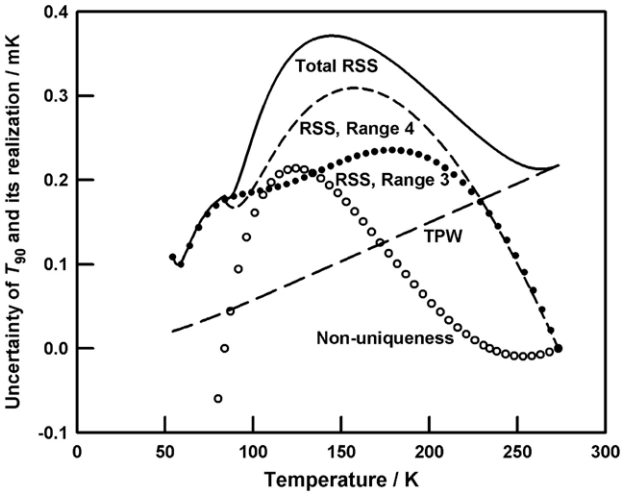

Figure 7. Propagated errors and uncertainty components ($k = 2$) for the SPRT realization of ITS-90 in the sub-ranges 54.3584 K to 273.16 K (SR 3) and 83.8 K to 273.16 K (SR 4). Calculations below 83.8 K are based on SR 3 and those above 83.8 K are based on SR 4. 'TPW' is the contribution from the realization of the triple point of water. 'Non-uniqueness' is the contribution from sub-range inconsistency (see section 3.).

4. Performance tests

In using equation (1) to calculate T/T_w, we assume that the microwave and acoustic eigenvalues are independent of temperature and that the corrections to the measured frequencies are understood. The microwave and acoustic data contain redundant information that we use to test these assumptions, independent of the values of T/T_w obtained using different modes. Here, we report consistency tests of the microwave frequency and half-width data. Next, we mention the small anisotropy of the thermal expansion of the resonator indicated by the microwave data. Finally, we report consistency tests of the acoustic frequency and half-width data.

4.1. Consistency of the microwave data

4.1.1. Frequency ratios among microwave triplets. In effect, the microwave frequency ratios provide the temperature dependence of the average radius, $\langle a \rangle$, of the quasi-sphere through the relation

$$\Re(T) \equiv \frac{\langle a(T) \rangle}{\langle a(T_w) \rangle} = \frac{\langle f_m + g_m \rangle_{T_w}}{\langle f_m + g_m \rangle_T}, \qquad (6)$$

Table 5. Principal uncertainty components ($k = 2$) for the SPRT realization of ITS-90 for each of the temperatures compared in this work.

T_{90}/K	U_c/mK	U_{wtp}/mK	U_{nu}/mK	U_{90}/mK	$U_{90}T_{90}^{-1}$/ μK K^{-1}
231.0	0.17	0.19	0.00	0.26	1.1
192.1	0.28	0.16	0.08	0.33	1.7
161.4	0.31	0.12	0.15	0.37	2.3
149.6	0.31	0.11	0.18	0.37	2.5
128.0	0.28	0.09	0.21	0.36	2.8
96.4	0.18	0.06	0.13	0.23	2.4
83.8	0.18	0.05	0.00	0.1	2.2
77.66, 77.86	0.17	0.04		0.17	2.2

Table 6. Calibration temperatures and uncertainties in millikelvin for the calibration of RIRT A129 from the NIST ICVGT realization.

Component	5.0 K	13.8 K	24.556 K
Type A statistics	0.031	0.048	0.052
Type B			
Resistance measurement	0.003	0.007	0.011
Resistance standard	0.004	0.011	0.022
Self-heating correction	0.011	0.011	0.015
ICVGT realization	0.042	0.108	0.170
RIRT transfer and interpolation	0.056	0.062	0.068
Thermal equilibrium	0.010	0.014	0.030
Combined Type B	0.072	0.127	0.187
Total standard uncertainty	0.078	0.135	0.194
Total expanded uncertainty ($k = 2$)	0.157	0.271	0.388

Table 7. Total expanded uncertainties U_{90} for RIRT A129 at temperatures compared in this work.

T_{90}/K	U_{90}/mK	$U_{90}T_{90}^{-1}$/μK K^{-1}
7.0	0.20	28
10.3	0.24	23
13.9	0.27	20
19.6	0.32	16
24.55	0.39	16

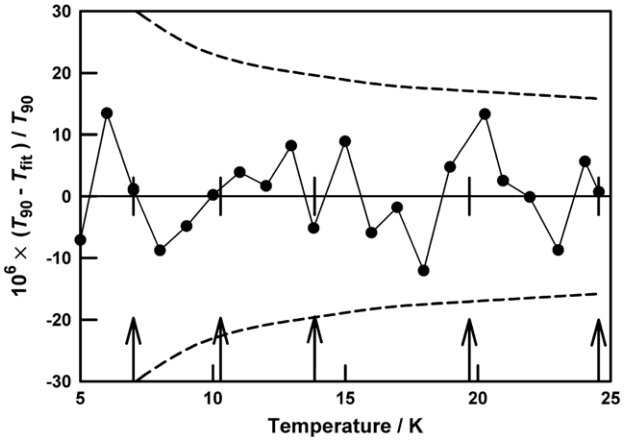

Figure 8. Residuals for the polynomial representation of the ICVGT realization on RIRT A129. The dashed curves are the total expanded ($k = 2$) uncertainty bounds. The arrows indicate the temperatures used in this work.

where the brackets '⟨⟩' indicate the average over the three components of one microwave triplet. Ideally, every microwave triplet would yield identical values of $\Re(T)$ and the values of $\Re(T)$ would not depend upon assumptions concerning the temperature-dependent resistivity of copper.

In [19], the frequencies and half-widths of each component of the TM11, TE11 and TM12 modes of the present resonator were measured at 277 K and 77 K and the data were used to calculate $\Re$ (277 K)/$\Re$ (77 K). The values of $\Re$ (277 K)/$\Re$ (77 K) for the three triplets had a standard deviation of 0.8 ppm from their mean. The mean value of $\Re$ (277 K)/$\Re$ (77 K) was 1.2 ppm larger when computed using g_{meas} than when computed using g_{calc}, using the $\sigma(T)$ data from [37] for OFHC copper with a residual resistance ratio of 300.

After [19] was completed, we reduced the coupling of the microwave probes to the cavity to reduce the microwave power dissipated in the quasi-sphere and the temperature gradients caused by this dissipation at low temperatures. The reduced microwave coupling reduced the signal-to-noise ratio of the TM12 mode so much that we stopped using it.

We acquired microwave data on every acoustic isotherm using the TM11 mode and deduced the radius ratio, $\Re(T)$ using g_{meas}. On six isotherms, we determined values of $\Re(T)$ separately using the TM11 and the TE11 modes. The difference $\Delta\Re \equiv \Re_{TM11} - \Re_{TE11}$ is a test of consistency that spans a factor of $f_{TE11}/f_{TM11} \approx 1.64$ in the microwave frequency. Averaged over the six isotherms, $\Delta\Re = (-0.5 \pm 1.9)$ ppm, where the uncertainty is one standard deviation.

4.1.2. Half-widths of microwave modes. We computed $\Re(T)$ from the TM11 mode data using both g_{meas} and g_{calc}, assuming a residual resistance ratio of 300 for g_{calc}. When g_{calc} was used, $\Re(T)$ was larger by 0.45 ppm at 83 K and 4.2 ppm at 7 K. In the uncertainty analysis (table 9), we treated this difference as an uncertainty contribution to $U(\Re)$. This contribution propagates into uncertainties of T/T_w (0.90 ppm at 83 K and 8.4 ppm at 7 K) that are much smaller than the uncertainties resulting from the inconsistencies among the acoustic modes above 77 K (section 4.2). If we had assumed that the residual resistance ratio was less than 300, the contribution to $U(\Re)$ from the microwave half-widths would be even smaller than the small values estimated here.

4.1.3. Evidence of anisotropic thermal expansion. The splittings of the three components of the microwave triplets had small temperature dependences. This is evidence of a small anisotropy of the thermal expansion of the assembled quasi-sphere. Following [23], we denote the components of the triplets 'x', 'y' and 'z' and we calculate the scaled fractional difference between the {frequency + halfwidth} of each component and the mean for the triplet (e.g. we compute $10^6[(f + g)_{TM11x}/\langle f + g\rangle_{TM11} - 1]$ for the x component of the TM11 mode). The three differences for the TM11 mode at T_w were −781.15, −366.69, 1147.84; upon cooling the quasi-sphere to 84 K, the differences decreased by 0.75, −1.70 and 0.95, respectively. The additional changes upon cooling to 7 K were negligible: 0.07, −0.14 and 0.07.

Assuming that the small temperature dependence of the microwave splittings results from anistropic thermal

expansion, the theory of the quasi-spherical cavity predicts that the splittings of the $(1, n)$ acoustic triplets have correspondingly small temperature dependences. Consistent with this, the values of $T/T_{\rm w}$ determined below from single components of the $(1, n)$ acoustic triplets agreed with the values of $T/T_{\rm w}$ determined with the isotropic $(0, n)$ acoustic modes.

The ability to detect anisotropic thermal expansion displayed here and in [1] demonstrates an advantage of measuring the thermal expansion of the cavity *in situ*. We might not have suspected anisotropy if we had inferred the thermal expansion of a cavity from auxiliary measurements made on samples of the material composing the cavity's walls.

4.2. *Internal consistency of the acoustic data*

On nearly every isotherm, we measured the frequencies and half-widths of five radially-symmetric modes [(0, 2), (0, 3), (0, 4), (0, 5), (0, 6)] and the frequency and half-width of a single component of three non-radial modes [(1, 3), (1, 4), (1, 5)]. We provide several demonstrations of the reliability of the data. Section 4.2.1 compares the measured values of the half-widths with the theory for the half-widths. Sections 4.2.2 and 4.2.3 demonstrate that, in the limit of zero pressure, the radial and non-radial modes give consistent results. Section 4.2.4 considers the degree of consistency of the radial modes at non-zero pressures. Section 4.2.5 demonstrates the repeatability of the measurements after an interval of four months. Finally, sections 4.2.6 and 4.2.7 demonstrate that the helium and the argon results are mutually consistent.

From the half-width test, we concluded that the data for (0, 2) and (1, 3) modes were unsatisfactory because the half-widths were much too large. We do not understand the cause of this problem; however, we recall that Benedetto *et al* [4] had a similar problem with the (0, 2) mode when they, like us, had a tuned gas-exhaust duct attached to the resonator. The frequency ratio test confirmed the unreliability of the (0, 2) and the (1, 3) data.

4.2.1. Excess half-widths of acoustic modes. Perturbation theory for a rigid, perfectly-isothermal, smooth-walled, acoustic cavity resonator of any shape predicts that $g_{\rm a}$ is a function of δ_T/L_T and $\delta_{\rm v}/L_{\rm v}$, where L_T and $L_{\rm v}$ are characteristic lengths of the cavity, δ_T is the thermal penetration length and $\delta_{\rm v}$ is the viscous penetration length. The penetration lengths are defined by

$$\begin{aligned} \delta_T^2 &\equiv \lambda/(\pi f \rho C_{\rm p}), \\ \delta_{\rm v}^2 &\equiv \eta/(\pi f \rho), \end{aligned} \tag{7}$$

where λ, η, ρ, $C_{\rm p}$ and f and are the thermal conductivity, viscosity, mass density, constant-pressure heat capacity and acoustic frequency, respectively. It is assumed that δ_T, $\delta_{\rm v} \ll L_T, L_{\rm v}$. Note also that the ratio of the lengths $\delta_{\rm v}/\delta_T = (Pr)^{1/2}$ exactly, where Pr is the Prandtl number.

For a spherical cavity of radius a, the perturbation theory result is

$$\left(\frac{\Delta f + {\rm i}g}{f}\right)_{\rm surface} = \frac{-1+{\rm i}}{2}\frac{\delta_T}{a} \times \left(\frac{\gamma - 1}{1 - l(l+1)/\xi_{l,n}^2} + \frac{\sqrt{Pr}}{-1 + z\xi_{l,n}/l(l+1)}\right), \tag{8}$$

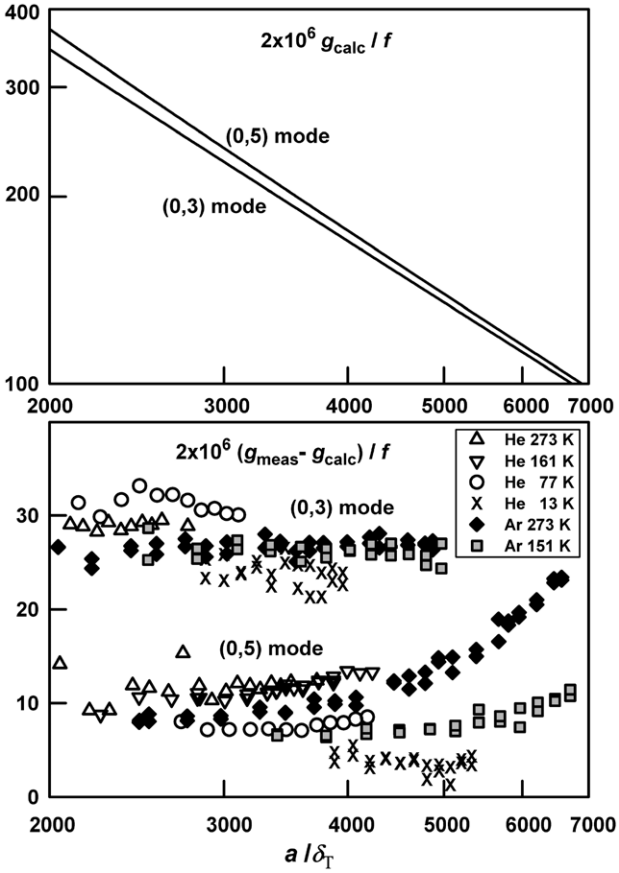

Figure 9. Top: theoretical half-widths for (0, 3) and (0, 5) acoustic modes scaled by $2 \times 10^6/f$. Bottom: Measured half-widths minus theoretical half-widths. For both panels, the horizontal axis is a/δ_T, the radius of the resonator divided by the thermal penetration length.

where $\xi_{l,n}$ is the eigenvalue for the mode (l, n) and $\gamma \equiv C_{\rm p}/C_{\rm V}$ is the heat capacity ratio [25]. In [19], an argument is made that the same perturbation approach applies to quasi-spheres, provided that the radius a is replaced with its mean value. In the limit of zero pressure, $\gamma - 1 = 2/3$, and throughout the temperature range of this work (7 K to 273 K) the Prandtl number of helium varies by only 0.3%: $0.6631 < (Pr)^{1/2} < 0.6649$ [21]. Thus, in the limit of zero pressure, the boundary contributions to $g_{\rm a,surface}$ are determined by only one ratio of lengths. We choose the ratio δ_T/a; one could equally well choose $\delta_{\rm v}/a$. The contribution to $g_{\rm a}$ from sound attenuation throughout the volume of a quasi-spherical cavity is

$$\frac{g_{\rm volume}}{f} = \left(\frac{\xi_{l,n}}{2}\frac{\delta_T}{a}\right)^2 \left[(\gamma - 1) + \frac{4}{3}Pr\right]. \tag{9}$$

We define the calculated half-width by $g_{\rm calc} \equiv g_{\rm surface} + g_{\rm volume}$. At low pressures, we expect that $g_{\rm calc}$ depends upon the properties of the working gas only through the ratio δ_T/a. Figure 9 displays the differences between the measured half-widths and the calculated half-widths, $\Delta g \equiv g_{\rm meas} - g_{\rm calc}$, for the (0, 3) and (0, 5) modes. The differences are scaled by $2 \times 10^6/f_{(0,n)}$, where $f_{(0,n)}$ is the resonance frequency. Figure 9 shows that, in the limit of small values of a/δ_T (which corresponds to low densities), $2\Delta g/f$ approaches 28 ppm for the (0, 3) mode and 9 ppm for the (0, 5) mode. These limits are

nearly independent of the temperature and also of whether the gas is helium or argon. This is a remarkable confirmation of the theory, considering the large variation of the gas properties spanned by the data ranging from 7 K to 273 K.

The values of $\Delta g/f$ in figure 9 are significantly larger than those reported in some previous acoustic studies of ITS-90 [1, 2]. This is of concern, because the same (unknown) phenomena that cause $\Delta g/f > 0$ might generate frequency perturbations that are of the order $\Delta g/f$. However, such frequency perturbations are likely to have pressure dependences that parallel those of $\Delta g/f$; therefore, they will also be a function of a/δ_T but not otherwise a function of the temperature. Accordingly, we consistently acquired data in the range $2000 < a/\delta_T < 5000$ and used them to extrapolate equation (1) to zero pressure (small values of a/δ_T). Because $\Delta g/f$ approaches a nearly temperature-independent value for each mode, we expected that the corresponding frequency perturbations would also approach a nearly temperature-independent value for each mode. To the extent that this is true, the frequency perturbations on the various isotherms cancel out the extrapolation to zero pressure. This approach of acquiring data in a consistent range of a/δ_T worked well. As shown in figure 1, our results for $(T - T_{90})/T_{90}$ agree with results acquired in other laboratories in the range 77 K to 273 K. Furthermore, the value $(T - T_{90})/T_{90} = -(60 \pm 4) \times 10^{-6}$ that we found using argon at 150 K agrees with the values of $(T - T_{90})/T_{90}$ that we determined on the nearby isotherms using helium.

When the values of $2\Delta g/f$ on the isotherms in figure 9 for the (0, 3) mode are extrapolated to zero pressure, they span a range of approximately 8×10^{-6}; the corresponding range for the (0, 5) mode is 4×10^{-6}. This degree of consistency across a wide temperature range is comparable to the degree of consistency of $2\Delta g/f$ for different modes at one temperature measured by others using resonators of similar sizes [4, 38]. We do not know any systematic way of converting this degree of consistency of $2\Delta g/f$ to an uncertainty in T/T_w. We note that equation (8) predicts equal mode-dependent values of $\Delta f_{surface}$ and $g_{surface}$. To the extent that our acoustic frequency data are inconsistent with equation (8), the values of T/T_w computed from various modes are inconsistent with each other. This inconsistency among the modes is listed in column 'U_r (acoustic)' of table 9 and it is a significant contribution to the uncertainty of T/T_w.

Figure 10 displays the excess half-widths of the (0, 3), (0, 4), (0, 5) and (0, 6) modes as a function of frequency. The points span all the temperatures and pressures encountered in this work. The peak in the data near 19 kHz is evidence that the breathing resonance of the copper quasi-sphere couples energy out of the radially symmetric acoustic modes. We did not use the data near 19 kHz in the determination of $(T - T_{90})$.

For completeness, we note that equation (9) overestimates $(\Delta f + ig)_{surface}$, because it neglects the penetration of the acoustic temperature oscillations into the copper wall bounding the cavity. Gillis *et al* [39] considered this problem near the liquid–vapour critical point and showed that the term $(\gamma - 1)$ in equation (9) should be replaced by $(\gamma - 1)(1 + \vartheta)^{-1}$, where

$$\vartheta^2 \equiv (\rho C_p \lambda)_{gas}/(\rho C_p \lambda)_{solid}. \qquad (10)$$

Often, the term $(1 + \vartheta)^{-1}$ is approximated by 1; in [40], it was approximated by $(1 - \vartheta)$. In this work, the largest values of ϑ are encountered at the lowest temperature (7 K) and the highest density (0.45 kg m^{-3}). Under these conditions, data from the literature [37, 21] lead to the estimate $100 < \vartheta < 650$, where the lower bound applies to copper with a residual resistivity ratio 40 and the upper bound corresponds to copper with a residual resistance ratio of 2000. Thus, the ϑ-dependent term in equation (10) is a small correction that decreases with the pressure. At 7 K, the effect of changing ϑ from 100 to ∞ on the value of $T - T_{90}$ is negligible compared with the other uncertainties from the acoustic measurements. This issue should be re-examined if acoustic thermometry is extended to much lower temperatures.

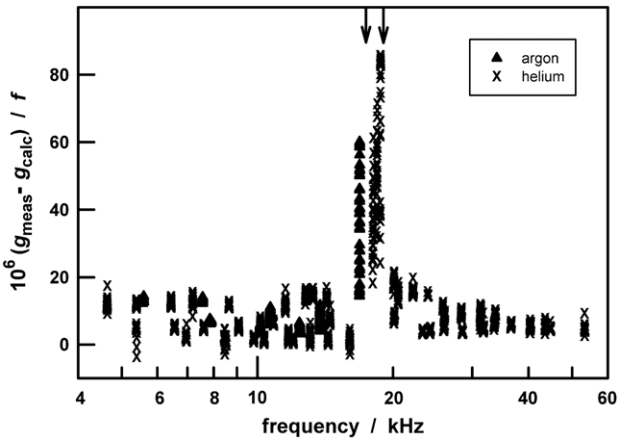

Figure 10. Scaled excess half-widths of the acoustic modes (0, 3), (0, 4), (0, 5) and (0, 6) at all the temperatures and pressures spanned by this work. The arrows at 19 kHz and 17.42 kHz indicate the frequency of the quasi-sphere's breathing resonance at T_w, as predicted by the thin-spherical-shell model and as fitted to the acoustic slopes β_a, respectively.

4.2.2. Frequency ratios of acoustic modes. Equation (1) assumes that the acoustic eigenvalues are independent of temperature. This assumption was tested on every isotherm by examining the zero-pressure limit of the square of the corrected frequency ratios

$$\Im \equiv \lim_{p \to 0} \left[\frac{f_a(T) + \Delta f_a(T)}{f_a(T_w) + \Delta f_a(T_w)} \right]^2 . \qquad (11)$$

The mean value of $\Im$, averaged over five or six modes, was used to compute T/T_w and the standard deviation from the mean of the five or six values is a contribution to the uncertainty of $T - T_{90}$, which appears in table 9 under the heading: $T \times U_r$(acoustic). Indeed, the inconsistency of the frequency ratios is the largest contribution to the uncertainty of $T - T_{90}$ in this work.

4.2.3. Consistent results from radial and non-radial modes. On every isotherm, we computed the mean value of $\Im$ (defined by equation (11)) separately averaged over the radial and the non-radial modes. We then computed the scaled differences $G \equiv 10^6(\langle\Im\rangle_{radial}/\langle\Im\rangle_{non\text{-}radial} - 1)$. The results for the radial and non-radial modes are indistinguishable, as shown in table 8.

Table 8. Comparison of frequency ratios for radial and non-radial acoustic modes.

T/K	G/ppm	$U(G)$/ppm
234.3120	−0.9	0.3
192.0895	1.5	2.4
161.3951	1.4	1.5
127.5580	9.2	2.8
96.4105	2.4	0.5
83.8012	0.5	1.1
77.8573	−1.6	0.6
77.6573	−1.7	1.0
24.5512	−0.2	0.2
19.6798	−1.2	0.3
13.8375	−1.0	0.2
10.2932	−0.2	0.1
7.0055	1.6	0.3
149.6832[a]	−1.0	2.6

[a] argon.

4.2.4. Consistency of acoustic modes at non-zero pressure. The determination of T/T_w requires only the zero-density limits of the speed of sound (equation (1)). However, a study of the pressure dependence of the speed of sound $u(p)$ can strengthen our confidence in the apparatus and the models used to analyse the data. Furthermore, an understanding of $u(p)$ is essential if a quasi-spherical cavity resonator is to be used as an interpolating acoustic gas thermometer (IAGT) over a wide temperature range, e.g. 4 K to 77 K. If a cavity is used as an IAGT, time and money will be saved if the microwave and acoustic resonance frequencies can be reliably extrapolated to zero pressure after being measured at one convenient pressure at each temperature of interest.

Conventionally, the pressure dependence of the speed of sound is represented by the acoustical virial expansion:

$$u^2 = u_0^2(1 + A_1 p + A_2 p^2 + \cdots). \tag{12}$$

(Here, u_0 is the zero-pressure limit of the speed of sound, $A_1 \equiv \beta_a/(RT)$ and $A_2 \equiv \gamma_a/(RT)$, where β_a and γ_a are the temperature-dependent acoustic virial coefficients [1].) We tested the consistency of values of A_1 determined for helium and for argon at T_w using several radially-symmetric resonance modes. This consistency test requires an understanding of how the elasticity of the wall of the quasi-spherical cavity changes the resonance frequencies of the gas within it.

The elasticity of a thin, spherical shell of thickness t enclosing a gas-filled spherical cavity of radius a reduces the frequencies of the $(0, n)$ acoustic modes by the amount $\Delta f_{\text{elastic}}$ (see equation (87) from [25]):

$$\frac{\Delta f_{\text{elastic}}}{f_{(0,n)}} \approx \frac{\kappa p}{1 - (f_{(0,n)}/f_{\text{breath}})^2} \tag{13}$$

with

$$\kappa = 5a/(6t\rho_{\text{shell}}u^2_{\text{shell}}). \tag{14}$$

Here, f_{breath} is the frequency of the radially-symmetric resonance of the empty spherical shell and the derivation of equations (13) and (14) assumed that the gas obeyed the ideal-gas equation of state with the specific-heat ratio $\gamma = 5/3$. Equations (12) and (13) imply that A_1 has the frequency-dependent correction $2\kappa[1 - (f_{(0,n)}/f_{\text{breath}})^2]^{-1}$

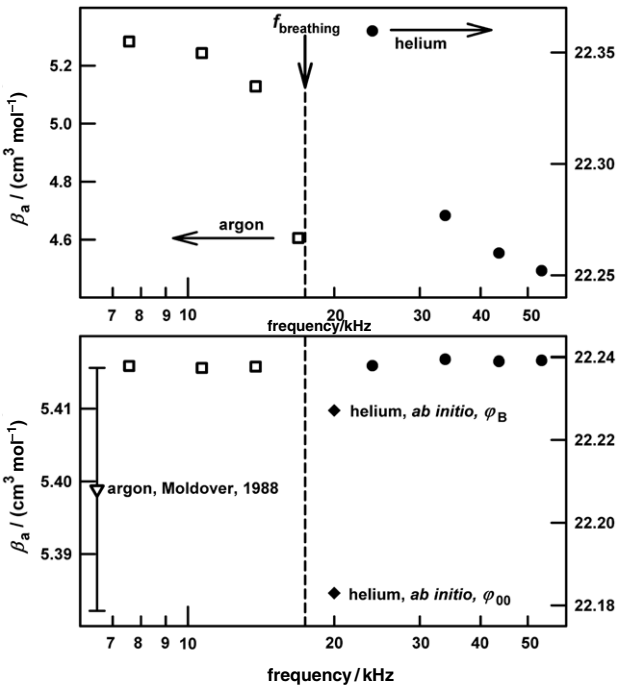

Figure 11. Acoustic slopes β_a before (top) and after (bottom) applying correction for the shell's elasticity. The scales on the left apply to argon (▽ [41], □ this work); the scales on the right apply to helium (♦ [21], ● this work).

where κ is given by equation (14); therefore, the elastic correction to A_1 has the weak temperature dependences of f_{breath} and $(\rho u^2)_{\text{shell}}$. Similarly, $\beta_a \equiv RTA_1$ has the frequency-dependent correction $2\kappa RT[1 - (f_{(0,n)}/f_{\text{breath}})^2]^{-1}$. Thus, the importance of the elastic correction to the determination of β_a varies approximately as T. At T_w, we estimated the parameters in the elastic correction ($f_{\text{breath}} = 19.31$ kHz, $\kappa = 2.7 \times 10^{-11}$ Pa^{-1}) from the dimensions of the resonator ($a = 5$ cm, $t = 1$ cm) and the density and the elastic constants of copper [37]. The model leading to these numerical estimates neglects the small quasi-spherical shape perturbations, the seam between the quasi-hemispheres, the bolts holding the quasi-hemispheres together and the objects attached to and supporting the quasi-hemispheres (cables, transducers, thermometers, gas inlet and outlet lines).

Before applying the elastic correction, the apparent values of $\beta_a(T_w)$ for helium and argon were mode-dependent, as indicated by the top panel of figure 11. After applying the correction using the fitted parameters $f_{\text{breath}} = 17.42$ kHz and $\kappa = 2.3 \times 10^{-11}$ Pa^{-1}, we found $\beta_a(T_w) = (5.4157 \pm 0.0001)$ cm^3 mol^{-1} for the $(0, 3)$, $(0, 4)$ and $(0, 5)$ modes of argon and $\beta_a(T_w) = (22.2389 \pm 0.0007)$ cm^3 mol^{-1} for the $(0, 3)$, $(0, 4)$, $(0, 5)$ and $(0, 6)$ modes of helium. The uncertainties are the standard deviations from the mean; thus, they indicate the consistency of the values of $\beta_a(T_w)$. We identified four additional sources of uncertainty of $\beta_a(T_w)$: (1) the thermal diffusivities of the gases, (2) $\gamma_a(T_w)$, (3) the microphones and (4) the calibration of the pressure transducer. We estimated that the microphones' compliances are the most important of these and that a 10% uncertainty of the compliances propagates into a 0.005 cm^3 mol^{-1} uncertainty of $\beta_a(T_w)$. The fitted parameter $f_{\text{breath}} = 17.42$ kHz coincides

with a resonance frequency of the shell that was independently observed during preliminary experiments using two PZT transducers that had been temporarily fastened outside the quasi-spherical shell. These experiments also detected shell resonances at 12.25 kHz and 21.05 kHz; however, they did not detect a resonance at the predicted frequency $f_{\mathrm{breath}} = 19.31$ kHz.

The lower panel of figure 11 shows that the corrected values of $\beta_{\mathrm{a}}(T_{\mathrm{w}})$ for helium and argon agree with the helium value computed from an *ab initio* helium–helium potential [21] and with the argon value measured using a 3 L, spherical, steel cavity [41]. This agreement and the small spread among the values of $\beta_{\mathrm{a}}(T_{\mathrm{w}})$ demonstrate that the thin-spherical-shell model for the elastic correction is relevant to the present quasi-spherical resonator, provided f_{breath} and κ are fitted to the data.

When fitting f_{breath} and κ at T_{w} we omitted the $(0,6)$ mode of argon because its frequency was close to f_{breath} (figure 11, top). Whenever any gas resonance is close f_{breath}, the elastic perturbation diverges according to equation (13). The divergence is a symptom of the failure of perturbation theory whenever the perturbation becomes large. A non-perturbative model for the coupling of two harmonic oscillators (such as a gas mode and a shell mode) will predict an avoided crossing instead of a divergent perturbation. Rather than dealing with the complexities of such a model, we avoid using gas modes for metrology whenever they occur at frequencies close to shell resonances.

If a quasi-spherical resonator is to be used as an IAGT over a wide temperature range, e.g. 4 K to 77 K, equation (12) implies that the uncertainty of product $\beta_{\mathrm{a}}(T)\rho_{\mathrm{gas}}(T)$ must be smaller than the desired uncertainty of the temperature. As an example, we consider this product for helium at the density 300 mol m^{-3}. We used the fitted values $f_{\mathrm{breath}}(T_{\mathrm{w}})$ and $\kappa(T_{\mathrm{w}})$ together with the approximations $f_{\mathrm{breath}}(T) \propto u_{\mathrm{copper}}/a$ and $\kappa(T) \propto (\rho u^2)_{\mathrm{copper}}$ to estimate $f_{\mathrm{breath}}(T)$ and $\kappa(T)$. The estimate used the published density and elastic constants of copper [37] and the values of $a(T)$ deduced from our microwave measurements. After applying the elasticity correction, we found that the standard deviation of the values of β_{a} was largest (0.01 cm^3 mol^{-1}) on the isotherm at 161 K. An uncertainty of 0.01 mol cm^{-3} in β_{a} corresponds to an uncertainty of the product $U(\beta_{\mathrm{a}}\rho_{\mathrm{helium}}) \approx 3 \times 10^{-6}$. This is small enough that other uncertainties are likely to dominate the performance of an IAGT.

We did not study the consistency of the values of β_{a} deduced from the $(1,n)$ modes, because we had data for, at most, three $(1,n)$ modes.

4.2.5. Redundant helium isotherms at 273 K. The 273.16 K isotherm for helium was measured on two occasions separated by four months. The first measurement was preliminary; it yielded useful data for the $(0,3)$, $(0,4)$, $(0,5)$, $(1,3)$ and $(1,4)$ modes. The second measurement benefited from our experience; it yielded more precise data for the same modes and also useful data for the $(0,6)$ mode. For these two measurements, the average value of the corrected squared frequency ratios, in the limit of zero pressure (equation (11)) was $\Im = 1 - (0.8 \pm 3.4) \times 10^{-6}$. The $k = 1$ uncertainty resulted from the scatter among the five modes.

4.2.6. Argon/helium comparison at 273 K. With the resonator at 273 K, we measured acoustic isotherms using both helium and argon. To avoid cross contamination of these gases, we evacuated the resonator ten times whenever we changed gases. Then we flushed the resonator at the rate 100 µmol s^{-1} for 60 h. In the limit of zero pressure, the square of the speed-of-sound ratio was $(u_{\mathrm{helium}}/u_{\mathrm{argon}})^2 = 9.980\,356 \pm 0.000\,022$. The stated uncertainty is the standard deviation of the values determined using the $(0,3)$, $(0,4)$, $(0,5)$, $(0,6)$, $(1,4)$ and $(1,5)$ modes. The small value of the uncertainty confirms that no gross errors were made in determining the zero-pressure limits of the acoustic frequencies on the crucial helium isotherm at T_{w}.

The ratio $(u_{\mathrm{helium}}/u_{\mathrm{argon}})^2$ is (10.2 ± 2.2) ppm smaller than the ratio expected from the molecular weights of commercial argon ($\mathrm{MW}_{\mathrm{argon}} = 39.947\,78$ g mol^{-1} [41]) and pure ^{4}He ($\mathrm{MW}_{\mathrm{helium}} = 4.002\,602$ g mol^{-1} [42]). The ratio is consistent with helium containing either 2.5 ppm of neon or 1.1 ppm of argon or some combination of neon and argon. While helium was flowing through the cavity at 77 K and 80 kPa, we inserted an improvised liquid-helium-cooled cold trap in the supply manifold. The square of the resonance frequencies, averaged over six modes, increased by (8.42 ± 1.49) ppm. The uncertainty from this test (1.49 ppm of T) is included in the 'impurity' column of table 9 for the isotherms below 77 K. This increase is consistent with the argon and/or neon impurities in the helium supply freezing out in the cold trap before reaching the resonator. Whenever the resonator was below 77 K, the tube supplying the helium gas to the resonator passed through a portion of the cryostat that was cooled to 4.2 K. Thus, we expect that any neon and/or argon in the supply gas would solidify in the supply tube before reaching the resonator, and we analysed the data assuming that this had occurred.

4.2.7. Argon/helium comparison at 150 K and 95 K. We measured the acoustic isotherm of argon at 150 K from which we deduced the value $(T - T_{90})/T_{90} = -(60 \pm 4) \times 10^{-6}$. As shown in the lower part of figure 1, this value is in excellent agreement with our helium results and also with the results from the literature.

We attempted to measure the acoustic isotherm of argon at 95 K; we abandoned the attempt when we found values of $2\Delta g/f$ that were much larger than those at other temperatures (e.g. at 128 kPa and 95 K, $2 \times 10^6 \times \Delta g/f$ for the $(0,5)$ mode was 28; in contrast, a typical value was 10, as shown in figure 9.). Mehl and Moldover [43] showed that precondensation of a gas on solid surfaces leads to large values of $2\Delta g/f$ as the pressure approaches the saturated vapour pressure (213 kPa for argon at 95 K). In contrast to previous researchers, we did not polish the machined copper surfaces of the quasi-spherical cavity because we did not want to alter its shape. Perhaps precondensation on the rough surfaces of our cavity led to larger values of $2\Delta g/f$ in argon at 95 K than observed by Ewing and Trusler at similar pressures [3].

5. Determination of T/T_{w} and $T - T_{90}$

At every equilibrium state, we measured the temperature of the resonator, the pressure, the resonance frequencies and half-widths of one or two microwave triplets, the resonance

Table 9. Results for $(T - T_{90})$ and component uncertainties ($k = 1$) expressed in millikelvin.

T/K	$T - T_{90}$/mK	U_{90}/mK	$U_{\text{total}}(T)$/mK	$T \times U_r$(acoustic)/mK	Impurity/mK	$T \times U_r(\Re)$/mK	$\gamma_a(T)$/mK
				Helium			
234.31	-3.57 ± 0.52	0.13	0.49	0.30	0.34	0.21	
192.08	-6.51 ± 0.55	0.16	0.52	0.41	0.28	0.16	
161.39	-8.87 ± 0.44[a]	0.18	0.40	0.30	0.23	0.14	
127.55	-7.79 ± 0.81	0.18	0.79	0.76	0.19	0.12	
96.410	-5.61 ± 0.26	0.12	0.22	0.14	0.14	0.11	
83.801	-4.65 ± 0.57	0.09	0.56	0.54	0.12	0.10	
77.857	-3.96 ± 0.32	0.09	0.31	0.28	0.11	0.07	
77.657	-4.05 ± 0.23	0.09	0.21	0.17	0.11	0.07	
24.551	-0.83 ± 0.29	0.19	0.22	0.05	0.04	0.09	0.19
19.679	0.24 ± 0.27	0.16	0.21	0.08	0.03	0.05	0.19
13.837	0.46 ± 0.21	0.14	0.16	0.04	0.02	0.06	0.14
10.293	-0.01 ± 0.16	0.12	0.10	0.01	0.02	0.06	0.08
7.0055	-0.31 ± 0.11	0.10	0.05	0.04	0.01	0.03	
				Argon			
149.68	-8.91 ± 0.58	0.19	0.54	0.53		0.12	

[a] This uncertainty includes a 0.15 mK contribution from temperature gradients (section 2.4).

frequencies and half-widths of up to seven acoustic modes and many other parameters that monitored the operation of the apparatus. On each isotherm, data were acquired at 15 to 25 equilibrium states that were equally spaced in density. Above 77 K, the density range was 50 mol m^{-3} to 300 mol m^{-3}; below 77 K, the range was 120 mol m^{-3} to 400 mol m^{-3}. Because 234 K is the mercury fixed point, we gave this isotherm extra attention; we used 69 equilibrium states spanning the density range 66 mol m^{-3} to 345 mol m^{-3}.

It is impractical to tabulate here the raw data used to determine T/T_w because the data set is approximately 10^4 numbers, many of them with seven significant figures. Upon request, the authors will provide the data in spreadsheets. Also, the data will be posted on the internet [44].

The calculation of the temperature ratios from the data acquired on each isotherm uses the procedures and the equations in [1] and [41]. For convenience, the steps are numbered. Except for Step 7, the uncertainties resulting from these corrections were all smaller than the uncertainties resulting from the inconsistencies among the acoustic modes:

(1) The acoustic and microwave frequencies were converted from quasi-isotherms to exact isotherms, with negligible uncertainty. For example, the data for the 96.4105 K isotherm were acquired in the range 96.41 K to 96.47 K. The conversion from this range to exactly 96.4105 K accounted for the thermal expansion of the cavity resonator, the temperature dependence of the zero-pressure speed-of-sound and the temperature dependence of the acoustic virial coefficient β_a.

(2) The largest correction to acoustic frequencies comes from the thermo-acoustic boundary layer. As calculated from equation (8), this correction to the frequency is, fractionally, $\approx \delta_T/(3a)$; its values ranged from 70 ppm to 170 ppm. This correction required values for thermophysical properties in equation (9), namely, the thermal conductivity λ, viscosity η, density ρ, constant-pressure heat capacity C_p and heat capacity ratio $\gamma \equiv C_p/C_v$. We computed ρ, C_p and γ from the virial equation of state, including the second density virial coefficient $B(T)$ and the third virial coefficient $C(T)$. As mentioned above, $B(T)$, λ and η were obtained from the *ab inito* calculation by Hurly [45] using the helium–helium interatomic potential φ_B developed by Hurly and Moldover [21]. (The potential ϕ_B is in better agreement with the recent *ab initio* calculations [22] than the potential ϕ_{00} used by Hurly and Moldover.) The results are weakly sensitive to the values of $C(T)$; the values of $C(T)$ are computed without quantum corrections [45].

(3) The acoustic frequencies were corrected for the compliance of the breathing mode of the copper shell. This correction is discussed in section 4.2.4. On many isotherms, one resonance frequency of the gas happened to be to close to the frequency of the breathing mode or the frequency of a non-radial mode of the copper shell. In such cases, the gas resonance had a large, pressure-dependent excess half-width Δg and the data for that mode were discarded (see figure 10).

(4) The acoustic frequencies were corrected for the thermal accommodation length assuming that the thermal accommodation coefficient was exactly unity. The effects of relaxing this constraint are considered in section 6.

(5) A small correction was made to the acoustic frequencies for the seam between the halves of the quasi-sphere. This correction assumed that the two halves were separated by a crevice 0.5 µm wide.

(6) A pressure-dependent correction was made to account for the compliance of the acoustic transducers. For this, we used the manufacturer's value for the compliance and equation (2.37) from [41].

(7) The corrected frequency data for each mode were fitted by adjusting the parameters u_0^2 and A_1 (and A_2 for argon) on the right side of the equation:

$$\begin{aligned} &(2\pi/\xi_a)^2(f_a + \Delta f_a)^2(1 - A_2 p^2) = (u_0/a)^2(1 + A_1 p) \\ &\quad \text{(helium)}, \\ &(2\pi/\xi_a)^2(f_a + \Delta f_a)^2 = (u_0/a)^2(1 + A_1 p + A_2 p^2) \\ &\quad \text{(argon)}. \end{aligned} \tag{15}$$

(Here, u_0 is the zero-pressure limit of the speed of sound, $A_1 \equiv \beta_a/(RT)$ and $A_2 \equiv \gamma_a/(RT)$, where

β_a and γ_a are the temperature-dependent acoustic virial coefficients [1].) In equation (15), we used the acoustic eigenvalues ξ_a appropriate for a perfectly spherical cavity. When the ratio T/T_w is computed, these eigenvalues drop out. When applying equation (15) to helium, we represented $\gamma_a(T)$ by the empirical function

$$T^2 A_2/(\mathrm{MPa/K})^2 = -0.113 + 1338\,(T/\mathrm{K})^{-3/2} - 8800(T/\mathrm{K})^{-5/2}. \quad (16)$$

We determined the numerical coefficients in equation (16) by fitting the speed-of-sound data of Gammon [46] and selected data from Plumb [47]. Because these data sets extend to much higher densities than our own, they determine $A_2(T)$ more accurately than we can, even though the uncertainties of our speed-of-sound measurements are much smaller. From the standard deviation of the fit, we estimated the uncertainty of $A_2(T)$ in the range 7 K to 24 K is 0.8 $(T/\mathrm{K})^2\,\mathrm{MPa}^{-2}$. This uncertainty is significant; its effects are included in table 9.

Typical deviations from fitting equation (15) are shown in figure 12. At the lowest densities, the deviations appear to be random; they result from the noise in the determination of the acoustic resonance frequencies. At higher densities, the deviations from the different modes are correlated (e.g. compare the (0, 4) and (1, 4) modes near 250 mol m^{-3} in figure 12). These deviations resulted from small errors in the measurement and control of the temperature.

The deviations from fitting equation (15) at 7 K were obviously pressure-dependent. For the 7 K isotherm, we refitted the acoustic data ignoring equation (16) and including $A_2(7\,\mathrm{K})$ as a fitting parameter. The result was $A_2(7\,\mathrm{K}) = (-0.15 \pm 0.05)\,\mathrm{MPa}^{-2}$. In contrast, equation (15) yields $A_2(7\,\mathrm{K}) = 0.09\,\mathrm{MPa}^{-2}$. Perhaps at 7 K, the term $A_3 p^3$ was large such that Plumb's value of $A_2(7\,\mathrm{K})$ had an undetected bias (here $A_3/(RT) \equiv \delta_a$ is the third acoustic virial coefficient).

Equation (17) for argon ignores the term $A_3 p^3$. Using data from the literature, we estimated that the maximum values of $A_3 p^3$ on our isotherms were 1.6×10^{-6} at 273 K and 1.1×10^{-6} at 150 K.

(8) The fitted values of $(u_0/a)^2$ for each mode at T and at T_w were combined with the microwave values of the squared radius ratio $\Re(T/T_w)$ to calculate T/T_w using equation (1). The values of $[(u_0/a)_T/(u_0/a)_{T_w}]^2$ differed for the various modes; their standard deviations are listed in table 9 under the heading '$T \times U_r$(acoustic)'. This is the largest uncertainty in T/T_w.

(9) Finally, the measurements of T/T_w and T_{90} were combined to determine $T - T_{90}$. The results are listed in table 9.

6. Discussion

6.1. Uncertainties of $(T - T_{90})$

Table 9 lists the values of $(T - T_{90})$, their total uncertainty ($k = 1$) and the largest components of their uncertainty. The column U_{90} accounts for the uncertainty of the realization of T_{90} and for the non-uniqueness of T_{90} (section 3). The column headed

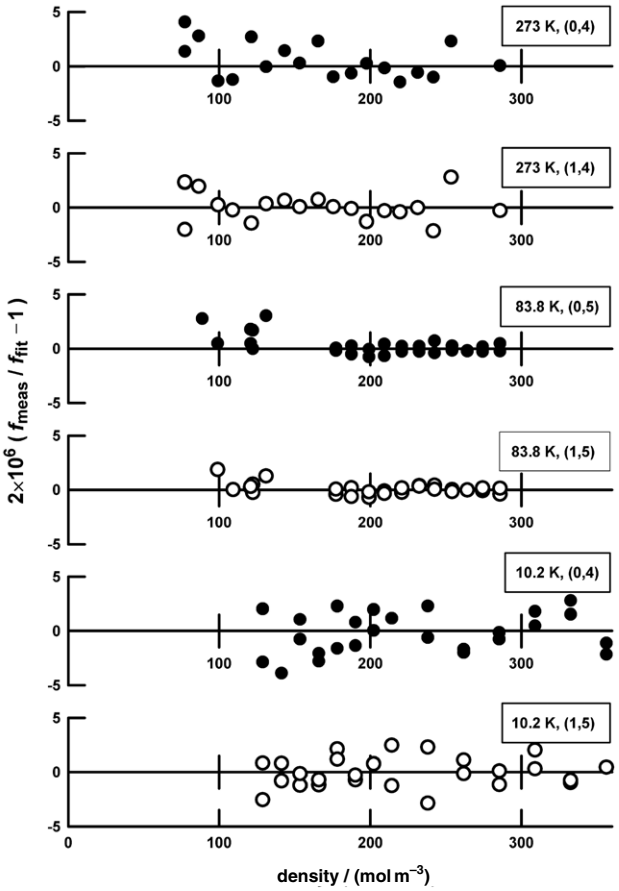

Figure 12. Typical deviation plots from fitting equation (15) to acoustic isotherms.

$U_{\mathrm{total}}(T)$ is the RSS of all of the columns to its right. It accounts for all the uncertainties in determining the thermodynamic temperature T. The column headed '$T \times U_r$(acoustic)' is the standard deviation of the values of ratio $(u_0/a)^2_T/(u_0/a)^2_{T_w}$ from their mean value. The mean and standard deviation were computed using at least five acoustic modes at T and T_w (section 4.2.2). The column headed 'impurity' accounts for possible impurities in the helium (sections 2.5 and 4.2.6). The column headed $T \times U_r(\Re)$ is the relative uncertainty of $(a_T/a_{T_w})^2$, the square of ratio of the average radius of the resonator at the temperature T to the average radius at the temperature T_w (section 4.1). It includes contributions that account for the uncertainty of the microwave penetration length, the inconsistencies among the microwave modes and the noise in the microwave data. The column labelled '$\gamma_a(T)$' accounts for how the higher virial coefficients of helium influence the extrapolation to zero pressure (section 5, Step 7). We now consider less important contributions to the uncertainties.

We estimated the contribution to the uncertainty of T/T_w from the uncertainty of the thermal conductivity λ of helium by refitting the isotherms after incrementing λ by its uncertainty. The largest effect was only 1.5 ppm on our 19 K isotherm. For this estimate, we used the values $U_r(\lambda)$ in table 6 of Hurly and Moldover which range from 1.7% at 5 K to 0.062% at 300 K [21]. This estimate is conservative because it does not account for the improved *ab intio* calculations of λ that we used.

The imperfections of the pressure transducer, including its zero-drift, made negligible contributions to the uncertainty of T/T_w.

In recent acoustic thermometry, values of the thermal accommodation coefficient $h \equiv 1$ [1], $h = 0.9$ [2] and $h = 0.82$ [3] were used, independent of the temperature, and in [4], h was a fitted parameter on each isotherm. In these cases, argon was interacting with polished stainless steel [1,2] or aluminum [3] surfaces. In section 5, Step 4, we assumed that the accommodation coefficient of helium interacting with a rough copper surface equals 1, exactly. Here, we conduct three tests that relax the constraint $h \equiv 1$. First, we refitted selected helium isotherms using equation (11) with the addition of the term $(A_{-1}\,p^{-1})$ that allows $h \neq 1$. In every case the additional term was not statistically significant; however, the uncertainty of $(T - T_{90})$ increased by at least a factor of 10 (for 273 K, 234 K, 95 K and 10.3 K, $T \times U_r$(acoustic) became 3.48 mK, 2.71 mK, 1.05 mK, 0.23 mK, respectively). Previous authors, including one of us (MRM), have used this test to estimate the uncertainty of $(T - T_{90})$ resulting from possible variations of h. We believe that this test overestimates the uncertainties associated with h, because h originates in the helium–copper interaction and we expect this interaction to be a smooth function of the temperature.

In a second test, we refitted the same isotherms, changing the constraint $h = 1$ to $h = 0.8$ at all temperatures (from [3] it was found that $\langle h \rangle = 0.82$). This changed $(T - T_{90})$ at 234 K, 95 K and 10.3 K from −3.57 to −3.48 mK, from −5.60 to −5.54 mK and from −0.01 to −0.00 mK, respectively. In the third test, we imposed the constraints $h = 1$ at 273 K and $h = 0.8$ at 10.3 K. This changed $(T - T_{90})$ at 10.3 K from −0.01 to −0.02 mK. In the second and third tests, the h-dependent changes in $(T - T_{90})$ were small compared with the total uncertainties of $(T - T_{90})$ listed in table 9. The weak h-dependence of $(T - T_{90})$ occurs, in part, because the present data span approximately the same density range on every isotherm. Although the thermal accommodation length varies inversely as the density, it increases only by a factor of 1.3 when the density is kept constant (e.g. 200 mol m^{-3}), while the temperature is increased by a factor of 39 (from 7 K to 273 K).

6.2. Comparisons with DCGT results

Figure 3 compares the present $(T - T_{90})$ results in the range 5 K to 25 K with the results that Fellmuth *et al* [5] derived by re-analysing the DCGT data taken at the PTB by Luther *et al*. We computed the $k = 1$ uncertainty bars for the PTB data in figure 3 by combining (as RSSs) the standard uncertainty U_{DCGT} of their DCGT determination with the standard uncertainty U_{90} of their T_{90} realization. As discussed in Fellmuth *et al* [5], $U_{DCGT}(T) = [0.3 + (0.3/23) \times (T/\text{K} - 4\text{ K})]$ mK. For the PTB realization of ITS-90 in this range, we used the constant $U_{90} = 0.15$ mK. The present $(T - T_{90})$ results agree remarkably well with the PTB results.

6.3. Comparisons with AGT results

In section 1.1 and figure 1, we compared the present acoustic gas thermometry with other recent acoustic gas thermometry (AGT). In the range 120 K to 380 K, all the AGT data sets are in mutual agreement within combined $k = 1$ uncertainties claimed by the various authors. As the temperature is reduced from 120 K, the present data and those of Ewing and Trusler [3] tend to diverge from each other and at 90 K the differences reach approximately 1.4 times the combined $k = 1$ standard uncertainties. Often, the differences between data sets from different laboratories are larger. In this case, we believe that the difference merits further study because (1) 90 K is near the lowest temperature where argon can be used in an AGT and (2) the agreement among the AGT data sets at higher temperatures appears to be better.

6.4. Fixed points

The results in Table 9 include new values for $(T - T_{90})$ essentially at the triple points of mercury T_{Hg} and argon T_{Ar} and values for $(T - T_{90})$ close to the triple points of neon T_{Ne} and equilibrium hydrogen $T_{e\text{-}H_2}$. This allows a re-determination of this series of fixed point temperatures T_{FP} that are traceable to particular NIST-maintained fixed point cells, independent of ITS-90 defined interpolations. In the case of neon and equilibrium hydrogen, we assumed that the differences $(T - T_{90})$ measured at the resonator's temperatures are the same as the differences $(T_{FP} - T_{90})$ that would have been measured if the measured isotherms were exactly at the fixed point temperatures. We now compare the present values of T_{FP} with other recent determinations.

6.4.1. The e-H_2 triple point. Our determination of $T_{e\text{-}H_2}$ is based on the NIST realizations of the e-H_2 TP and an ICVGT as carried on RIRT A129. This RIRT has not been calibrated directly with an e-H_2 TP cell; instead, it carries a calibration derived only from the ICVGT realization at NIST [32]. The ICVGT is, in turn, calibrated at three ITS-90 fixed point temperatures, the e-H_2 TP, the Ne TP and a ^{4}He vapour pressure point. While the RIRT interpolation equation gives ICVGT temperatures, these temperatures will not necessarily agree exactly with the e-H_2 TP realization temperature because of uncertainties in the ICVGT pressure measurement. We avoided these additional uncertainties by utilizing the multiple comparison measurements made between RIRT A129 and RIRT B174 that establish a direct link to the NIST e-H_2 TP cell H_2-212 [34]. The residual of the ICVGT fit for RIRT A129 is −0.07 mK at 13.8 K (see figure 6). However, there is a fortuitous agreement between the interpolated ICVGT temperature and the temperature corresponding to the plateau of H_2-212; the two differ by only 0.02 mK. Therefore, the calculation of $T_{e\text{-}H_2}(H_2\text{-}212)$ is based on the observed difference $T - T_{90}$ from table 9 with only a very small correction.

After making this correction, we obtain $T_{e\text{-}H_2}(H_2\text{-}212) = (13.803\,78 \pm 0.000\,17)$ K. The cell H_2-212 was part of a recent international-star intercomparison of triple point cells [48] and it contains hydrogen with the known deuterium-to-hydrogen concentration ratio $R_D = 29.1 \times 10^{-6}$, by mole fraction. This cell's plateau temperature can be corrected to the specific deuterium concentration ratio of 89.02 that is equivalent to that of the isotope reference material: Standard Light Antarctic Precipitation (SLAP) [49]. The correction is 0.325 mK, according to the recommended correction coefficient [50] of

5.42 K/R_D. The result is $T_{e\text{-}H_2}(H_2\text{-'SLAP'}) = (13.804\,10 \pm 0.000\,17)$ K.

Within the combined standard uncertainties, our value of $T_{e\text{-}H_2}(H_2\text{-'SLAP'})$ agrees with the value (13.8039 ± 0.0005) K reported by Rusby *et al* [51] based on the re-analysis of the DCGT data of Luther *et al* by Fellmuth *et al* [5].

6.4.2. The Ne triple point. Our determination of T_{Ne} is based on the NIST realizations of the Ne TP and NIST realizations of the ICVGT as carried out on RIRT A129 in a way analogous to that of e-H_2 TP. Also, direct realizations of the NIST Ne TP are available using RIRT A129 with the cell Ne-201 that was a part of the recent international comparison of triple-point cells [52]. Unlike e-H_2, the NIST Ne TP cells do not exhibit perfectly flat plateau temperatures. Therefore, we extrapolated to the temperature corresponding to the $F = 100\%$ melted percentage (i.e. the liquidus point) using the melting data spanning the range $50\% < F < 95\%$. An additional complication in determining T_{Ne} is the apparent difference of (0.13 ± 0.02) mK between the Ne TP temperature as realized in the cell 'Ne-LTRF' by Meyer and Reilly [32] and the NIST reference cell 'Ne-201' [34]. For the ICVGT calibration carried on RIRT A129, the interpolated temperature corresponding to 24.5561 K is 0.12 mK higher than T_{Ne}(Ne-201).

After accounting for the considerations in the preceding paragraph, we obtained T_{Ne}(Ne-201) $= (24.555\,15 \pm 0.000\,25)$ K and T_{Ne}(Ne-LTRF) $= (24.555\,27 \pm 0.000\,26)$ K. These values can be compared with the average value $T_{DCGT} - T_{90} = 0.17$ mK near the Ne TP reported by Fellmuth *et al* [5] which implies T_{Ne}(DCGT) $= (24.556\,27 \pm 0.000\,57)$ K using the DCGT data. The apparent discrepancies of 1.1 mK and 1.0 mK are only 1.8 and 1.6 times the combined standard uncertainties for the measurements, respectively. Approximately half of this difference could be due to differences in T_{90} between NIST and PTB, such as those indicated by the results of the CCT KC-1 [33].

The Ne gas used to fill the cell Ne-201 was 99.9995% commercially purified neon. The isotopic composition of this neon is not known; however, we assumed that it was close to the recommended abundance fractions found in air [53]. Because recent evidence [54] indicates that commercial neon is substantially different in isotopic composition from the currently recommended abundance fractions, we assign a type B standard uncertainty of 0.08 mK to allow for the possible effects of isotopic variations.

6.4.3. The Ar triple point. Table 9 gives the temperature of the Ar TP, as determined in these measurements. The SPRT 1842382 was calibrated directly using the NIST argon cell Ar-NBS-3 [25]. This Ar TP is also realized by extrapolation to a liquidus point where $F = 100\%$ is the melted percentage. The difference in the realization temperature obtained via this cell and that of other NIST Ar TP cells is given in [29]. The present value T_{Ar}(Ar-NBS-3) $= (83.801\,15 \pm 0.000\,57)$ K can be compared with Astrov's 1995 value $T_{Ar} = (83.8072 \pm 0.0021)$ K [10]. The 6 mK difference is approximately three times the combined uncertainties.

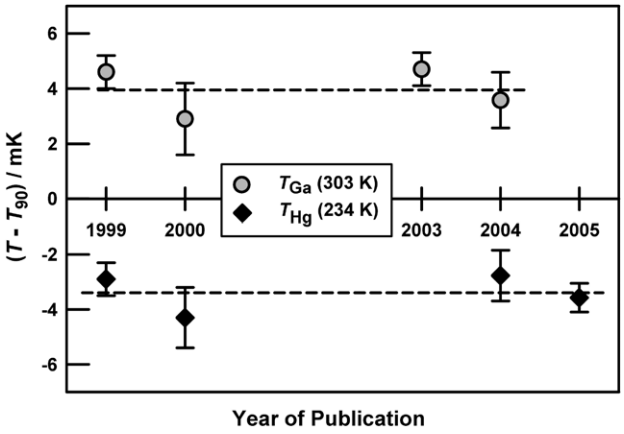

Figure 13. Recent acoustic determinations of $(T - T_{90})$ at the gallium and mercury points. The data sources by year are: 1999 [1]; 2000 [3]; 2003 [2]; [illegible] [4]; 2005, this work. The dashed lines indicate the unweighted averages: $(T - T_{90}) = (3.95 \pm 0.86)$ mK at T_{Ga} and $(T - T_{90}) = (3.39 \pm 0.70)$ mK at T_{Hg}. (The uncertainties are one standard deviation.)

6.4.4. The Hg triple point. Table 9 gives the temperature of the Hg TP. As mentioned above, our value for T_{Hg} is based on direct realizations with the NIST immersion Hg TP cell 'Hg-GC-1' [28] using the SPRT 1842382. Figure 13 compares our value for T_{Hg} with three other recent determinations of T_{Hg}. Remarkably, these four values determined by acoustic gas thermometry are in mutual agreement within combined $k = 1$ uncertainties. The unweighted average of these four values of T_{Hg} is $(T - T_{90}) = -(3.39 \pm 0.70)$ mK.

For completeness, figure 13 also compares four recent determinations of T_{Ga} that used acoustic gas thermometry. As is the case for T_{Hg}, the four values are in mutual agreement within combined $k = 1$ uncertainties. At T_{Ga}, the unweighted average of the acoustic gas thermometry data is $(T - T_{90}) = (3.95 \pm 0.86)$ mK.

6.5. The second acoustic virial coefficient β_a

In our analysis (section 5, Step 2), we used values of the thermal conductivity $\lambda(T)$ of helium that were calculated from the *ab initio* helium–helium interatomic potential φ_B. When discussing uncertainties (section 6.1), we estimated the uncertainty of $\lambda(T)$ as the difference between $\lambda(T)$ calculated from φ_B and $\lambda(T)$ calculated from the alternative potential φ_{00}. In figure 14, we test the reliability of φ_B by comparing the *ab initio* values of the second acoustic virial coefficient of helium β_a with the values of β_a in table 10 that we obtained from fitting equation (15) to the acoustic data. On the lower panel of figure 14, the baseline represents the values of β_a calculated from the potential φ_B and the dashed curve represents the values of β_a calculated from alternative potential φ_{00}. As in [21], the difference between the baseline and the dashed curve is an estimate of the uncertainty of the theoretical values of β_a. Remarkably, nearly all the measured values of β_a fall between the values from φ_{00} and from φ_B. Thus, nearly all the measurements are consistent with these potentials, within combined uncertainties. In figure 14, the uncertainty bars for $\beta - \beta_{calc}$ include five components added in quadrature that account for (1) the standard deviation of the values of

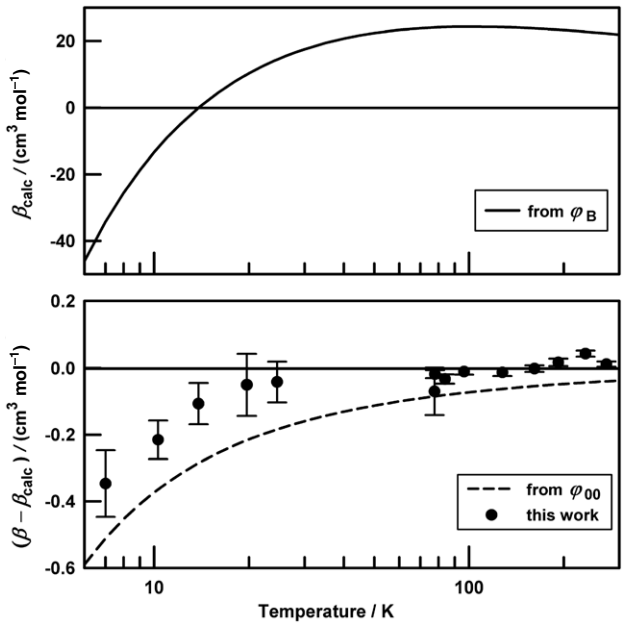

Figure 14. Top: second acoustic virial coefficients $\beta_a(T)$ calculated from the *ab initio* helium–helium potential φ_B. Bottom: comparison of measured and calculated values of $\beta_a(T)$ using a baseline calculated from φ_B. The dashed curve was calculated from the potential φ_{00}. The $k = 1$ uncertainty bars are discussed in section 6.5.

Table 10. Second acoustic virial coefficient β_a of helium calculated from φ_{00} and determined by fitting equation (15) to speed-of-sound data.

T/K	$\beta_{a,calc}$/cm^3 mol^{-1}	$\beta_{a,meas}$/cm^3 mol^{-1}
273.1600	22.227	22.239 ± 0.008
234.3156	22.753	22.796 ± 0.009
192.0960	23.364	23.413 ± 0.011
161.4040	23.772	23.769 ± 0.010
127.5658	24.171	24.149 ± 0.011
96.4161	24.281	24.270 ± 0.009
83.8058	24.177	24.132 ± 0.014
77.8613	24.061	24.030 ± 0.012
77.6613	24.057	23.976 ± 0.071
24.5520	14.415	14.368 ± 0.061
19.6796	9.959	9.885 ± 0.093
13.8300	−0.053	−0.178 ± 0.062
10.2934	−11.943	−12.221 ± 0.058
7.0057	−34.29	−34.64 ± 0.10

β_a from the various $(0, n)$ acoustic modes (section 4.2.4), (2) the uncertainty of $\gamma_a(T)$, (3) the uncertain compliance of the transducers (0.005 cm^3 mol^{-1}), (4) the uncertainty of f_{breath} and (5) the calibration of the pressure transducer. We plan to extend the acoustic measurements to higher pressures; we expect this will reduce the uncertainty from $\gamma_a(T)$ below 77 K.

6.6. Concluding remarks

We have demonstrated that an acoustic thermometer of moderate size functions as a precise, accurate primary thermometer spanning the temperature range 7 K to 273 K. Because we have determined $\beta_a(T)$ and soon will determine $\gamma_a(T)$, this instrument can be used to calibrate other thermometers at any desired temperature within its range without repeating the acoustic measurements on a complete isotherm. The uncertainties achieved are comparable to, or smaller than, those achievable using the ICVGT as currently defined on the ITS-90. It is likely that this instrument will provide useful results at even lower temperatures than those presented here, particularly if ^{3}He is used as the working fluid.

Acknowledgments

We thank Dean Ripple and Greg Strouse of the Thermometry Group of NIST for lending us the thermometers and the bridges that enabled us to measure the temperature of the resonator on the ITS-90. They also provided numerous suggestions for designing the apparatus and analysing the data. Eric May and Jim Mehl were particularly helpful in modelling and characterizing the quasi-spherical resonator. We thank John Hurly for providing tables of the thermophysical properties of helium derived from the helium–helium potential ϕ_B using the methods of [21]. Arnaud Richard prepared the drawings of the apparatus. This manuscript benefited from numerous improvements suggested by Dan Friend, Eric May and Dean Ripple.

References

[1] Moldover M R, Boyes S J, Meyer C W and Goodwin A R H 1999 *J. Res. Natl Inst. Stand. Technol.* **104** 11–46
[2] Strouse G F, Defibaugh D R, Moldover M R and Ripple D C 2003 *Temperature: its Measurement and Control in Science and Industry, 8th Int. Temperature Symp. (Chicago IL, 21–24 October, 2002)* vol 7 ed D C Ripple, pp 31–6 (*AIP Conf. Proc.* **684**)
[3] Ewing M B and Trusler J P M 2000 *J. Chem. Thermodynam.* **32** 1229–55
[4] Benedetto G, Gavioso R M, Spagnolo R, Marcarino P and Merlone A 2004 *Metrologia* **41** 74–98
[5] Fellmuth B, Fischer J, Gaiser C and Haft N 2004 *TEMPMEKO 2004: 9th Int. Symp. on Temperature and Thermal Measurements in Industry and Science (Dubrovnik, Croatia, 22–25 June 2004)* (preprint)
The above cited work reanalyses the data from Luther H, Grohmann K and Fellmuth B 1995 *Metrologia* **33** 341–52
[6] Mehl J B and Moldover M R 1986 *Phys. Rev.* A **34** 3341–4
[7] Martin J E, Quinn T J and Chu B 1988 *Metrologia* **25** 107–12
[8] Guildner L A and Edsinger R E 1976 *J. Res. Natl Bur. Stand.* A **80** 703–37
[9] Schooley J F 1990 *J. Res. Natl Inst. Stand. Technol.* **95** 255–90 and references therein
[10] Astrov D N, Belyansky L B and Dedikov Y A 1995 *Metrologia* **32** 393–5
This 1995 reference corrects the 1989 reference: Astrov D N, Beliansky L B, Dedickov Y A, Polunin S Pl and Zakharov A A 1989 *Metrologia* **26** 151–66
[11] Kemp R C, Kemp W R G and Besley L M 1986/87 *Metrologia* **23** 61–86
[12] Steur P P M and Durieux M 1986 *Metrologia* **23** 1–18
[13] Ernst G, Brauning G and Lai J-F 1988 *Can. J. Chem.* **66** 999–1004
[14] Hill K D 1995 *Metrologia* **32** 87–94
[15] Singh Y T, Maas H, Edler F and Zaidi Z H 1994 *Metrologia* **31** 49–50
[16] Rusby R L, Hudson R P, Durieux M, Schooley J F, Steur P P M and Swenson C A 1991 *Metrologia* **28** 9–18
[17] Berry K H 1979 *Metrologia* **15** 89
[18] Clark A F, Childs G E and Wallace G J 1970 Advances in cryogenic engineering *Proc. 1969 Cryogenic Engineering*

Conf. (Los Angeles, 16–18 June) ed K D Timmerhaus (New York: Plenum)
[19] Mehl J B, Moldover M R and Pitre L 2004 *Metrologia* **41** 295–304
[20] Ripple D C, Defibaugh D R, Moldover M R and Strouse G F 2003 Techniques for primary acoustic thermometry to 800 K *Temperature: its Measurement and Control in Science and Industry, 8th Int. Temperature Symp (Chicago IL, 21–24 October, 2002)* ed D C Ripple, pp 25–30 (*AIP Conf. Proc.* **684**)
[21] Hurly J J and Moldover M R 2000 *J. Res. Natl Inst. Stand. Technol.* **105** 667–88
[22] Cencek W, Jeziorska M, Bukowski R, Jaszuński M, Jeziorsi B and Szalewicz K 2004 *J. Phys. Chem.* A **108** 3211
[23] May E F, Pitre L, Mehl J B, Moldover M R and Schmidt J W 2004 *Rev. Sci. Instrum.* **75** 3307–17
[24] Richardson R C and Smith E N 1998 *Experimental Techniques in Condensed Matter Physics at Low Temperatures* (Redwood City, CA: Addison-Wesley) Figure 4.24(b)
[25] Moldover M R, Mehl J B and Greenspan M 1986 *J. Acoust. Soc. Am.* **79** 253–72
[26] Furukawa G T 1982 *Temperature: its Measurement and Control in Science and Industry, 6th Int. Temperature Symp. (Washington, D.C., 15–18 March, 1982)* vol 5 ed J F Schooley, pp 239–48 (New York: American Institute of Physics)
[27] Furukawa G T 1986 *J. Res. Natl Bur. Stand.* **91**, 255–75
[28] Strouse G F 1999 *TEMPMEKO '99: 7th Int. Symp. on Temperature and Thermal Measurements in Industry and Science (Delft, The Netherlands, 1–3 June, 1999)* ed J F Dubbeldam and M J de Groot (Delft, The Netherlands: NMi Van Swinden Laboratorium) pp 147–52
[29] Strouse G F and Lippiatt J 2002 *TEMPMEKO 2001: 8th Int. Symp. on Temperature and Thermal Measurements in Industry and Science (Berlin, Germany, 19–21 June, 2001)* ed B Fellmuth *et al* (Berlin: VDE Verlag) pp 453–8
[30] Meyer C W and Tew W L 2003 *Temperature: its Measurement and Control in Science and Industry, 8th Int. Temperature Symp. (Chicago IL, October 21–24, 2002)* vol 7, ed D C Ripple, pp 137–42 (*AIP Conf. Proc.* **684**)
[31] Meyer C W and Reilly M L 1996 *Metrologia* **33** 383–9
[32] Meyer C W and Reilly M L 1997 *Proc. TEMPMEKO '96: 6th Int. Symp. on Temperature and Thermal Measurements in Industry and Science (Torino, Italy, 10–12 September, 1996)* ed P Macarino (Torino: Levrotto and Bella) pp 39–44
[33] Rusby R L *et al* 2005 CCT Key Comparison No 1 (CCT-K1): Realizations of the ITS-90, 0.65 K to 24.5561 K, using rhodium–iron resistance thermometers *Proc. 9th Int. Symp. on Temperature and Thermal Measurements in Industry and Science, TEMPMEKO 2004 (Dubrovnic, Croatia, 22–25 June 2004)* ed D Zvizdic (Zagreb: FSB and LPM) pp 1031–6
[34] Tew L and Meyer C W 2003 *Temperature: its Measurement and Control in Science and Industry, 8th Int. Temperature Symp. (Chicago IL, 21–24 October, 2002)* vol 7, ed D C Ripple (*AIP Conf. Proc.* **684**) pp 143–8
[35] Meyer C W, Strouse G F and Tew W L 1999 *TEMPMEKO '99: 7th Int. Symp. on Temperature and Thermal Measurements in Industry and Science (Delft, The Netherlands, 1–3 June, 1999)* ed J F Dubbeldam and M J de Groot (Delft, The Netherlands: NMi Van Swinden Laboratorium) pp 89–94
[36] White D R 1997 *Proc. TEMPMEKO '96: 6th Int. Symp. on Temperature and Thermal Measurements in Industry and Science (Torino, Italy, 10–12 September, 1996)* ed P Macarino (Torino: Levrotto and Bella) pp 129–34
[37] Simon N J, Drexler E S and Reed R P 1992 *NIST Monograph 177: Properties of Copper and Copper Alloys at Cryogenic Temperatures* (Washington, US: Government Printing Office)
[38] Ewing M B, McGlashan M L and Trusler J P M 1986 *Metrologia* **22** 93–102
[39] Gillis K A, Shinder I I and Moldover M R 2004 *Phys. Rev.* E **70** 021201
[40] Gillis K A, Mehl J B and Moldover M R 2003 *J. Acoust. Soc. Am.* **114** 166–73
[41] Moldover M R, Trusler J P M, Edwards T J, Mehl J B and Davis R S 1988 *J. Res. Natl Bur. Stand.* **93** 85–144
[42] Coplen T B 2001 *J. Phys. Chem. Ref. Data* **30** 701–12
[43] Mehl J B and Moldover M R 1982 *J. Chem. Phys.* **77** 455–65
[44] http://www.cnam.fr/instituts/inm/acoustic-thermometry-nist-inm/data_acoustic_07_01_04to12_20_04.xls
[45] Hurly J J 2005 private communication
[46] Gammon B E 1976 *J. Chem. Phys.* **64** 2556
[47] Plumb H H 1982 *Temperature: its Measurement and Control in Science and Industry, 6th Int. Temperature Symp. (Washington, D.C., 15–18 March, 1982)* vol 5, ed J F Schooley (New York: American Institute of Physics) pp 77–88
[48] Fellmuth B *et al* 2005 *Metrologia* **42** 171–93
[49] Gonfiantini R 1978 *Nature* **271** 534–6
[50] Steur P P M, Hermier Y, Gam K S, Hill K D, Fellmuth B, Pokhodun A I and Ripple D C 2005 Bureau International de Poids et Mesures, Consultative Committee on Thermometry, CCT/05-06
[51] Rusby R, Moldover M R, Fischer J, White D R, Steur P P M, Hudson R P, Durieux M and Hill K D 2005 Bureau International de Poids et Mesures, Consultative Committee on Thermometry, CCT/05-19
[52] Fellmuth B *et al* 2003 *Temperature: its Measurement and Control in Science and Industry, 8th Int. Temperature Symp. (Chicago IL, 21–24 October, 2002)* vol 7, ed D C Ripple, pp 885–90 (*AIP Conf. Proc.* **684**)
[53] DeLaeter J R, Bohlke J K, De Bievre P, Hidaka H, Peiser H S, Rosman K J R and Taylor P D P 2003 *Pure Appl. Chem.* **75** 683–800
[54] Pavese F 2005 *Metrologia* **42** 194–200